Reliability of PV Modules:

Dependence on Manufacturing Quality and Field Climatic Conditions

by

Shantanu Pore

A Thesis Presented in Partial Fulfillment
of the Requirements for the Degree
Master of Science

Approved April 2017 by the
Graduate Supervisory Committee:

Govindasamy Tamizhmani, Co-Chair
Matthew Green, Co-Chair
Devrajan Srinivasan

ARIZONA STATE UNIVERSITY
May 2017

ABSTRACT

This is a two-part thesis assessing the long-term reliability of photovoltaic modules.

Part 1: Manufacturing dependent reliability - Adapting FMECA for quality control in PV module manufacturing

This part is aimed at introducing a statistical tool in quality assessments in PV module manufacturing. Developed jointly by ASU-PRL and Clean Energy Associates, this work adapts the Failure Mode Effect and Criticality Analysis (FMECA, IEC 60812) to quantify the impact of failure modes observed at the time of manufacturing. The method was developed through analysis of nearly 9000 modules at the pre-shipment evaluation stage in module manufacturing facilities across south east Asia. Numerous projects were analyzed to generate RPN (Risk Priority Number) scores for projects. In this manner, it was possibly to quantitatively assess the risk being carried the project at the time of shipment of modules. The objective of this work was to develop a benchmarking system that would allow for accurate quantitative estimations of risk mitigation and project bankability.

Part 2: Climate dependent reliability - Activation energy determination for climate specific degradation modes

This work attempts to model the parameter (Isc or Rs) degradation rate of modules as a function of the climatic parameters (i.e. temperature, relative humidity and ultraviolet radiation) at the site. The objective of this work was to look beyond the power degradation rate and model based on the performance parameter directly affected by the degradation mode under investigation (encapsulant browning or IMS degradation of solder bonds). Different physical models were tested and validated through comparing the activation energy obtained for each degradation mode. It was concluded that, for the degradation of the solder bonds within the module, the Pecks equation (function of temperature and relative humidity) modelled with Rs increase was the best fit; the activation energy ranging from 0.4 – 0.7 eV based on the climate type. For encapsulant browning, the Modified Arrhenius equation (function of temperature and UV) seemed to be the best fit presently, yielding an activation energy of 0.3 eV. The work was concluded by suggesting possible modifications to the models based on degradation pathways unaccounted for in the present work.

To,

My father, mother, and brother, for their unconditional love, unending support and unwavering belief in me.

I hope I do you'll proud.

ACKNOWLEDGMENTS

I would like to express my sincere gratitude to Dr. Govindasamy Tamizhmani, my guide and mentor, who has made all this possible. I consider myself immensely fortunate to have worked in your lab and benefitted from your insight and experience. Thank you for this opportunity to make this the most productive two years of my life. I would also like to thank the members on my panel, Dr. Green and Dr. Srinivasan, for their guidance and support along the way. It would be remiss of me to not mention the friends I have made along the way at ASU-PRL, who have played a key role in helping me build this research work. Firstly, Sai Tatapudi, less of a manager and more of a close friend, who contributed greatly through his insight. A big shout out to Darshan, Chris, Srinivas, Sushant, and Abhishiktha, who provided different perspectives on issues whenever required. Lastly, I would take this opportunity to thank all the former students of PRL whose work has laid the foundation for future generations to build upon. My research has been a humble attempt at continuing the work at PRL and repaying some of the faith everyone at PRL invested in me over the past two years.

TABLE OF CONTENTS

Page

CHAPTER Page

CHAPTER Page

LIST OF TABLES

Table Page

LIST OF FIGURES

Figure Page

Figure Page

PART 1

MANUFACTURING DEPENDENT RELIABILITY - ADAPTING FMECA FOR QUALITY CONTROL IN PV MODULE MANUFACTURING

1.1 INTRODUCTION

1.1.1 Background

Photovoltaic modules operating in the field can experience diverse types of failure modes, based on three governing factors – the climatic conditions, the electrical configurations, and the manufacturing quality. This part of the thesis focusses on the failure modes associated with quality at the time of manufacturing. At present, quality control during manufacturing is conducted largely by independent quality assurance firms present at the manufacturing locations on behalf of the client. One aspect of quality control is pre- shipment evaluation wherein randomly selected modules from ready lots are evaluated through tools such as visual inspection, flash testing and electroluminescence imaging. The pre-shipment evaluation data of approximately 90000 modules of similar general construction: glass – polymer – cell – backsheet, was made available by a quality assurance firm for the work outlined hereafter.

This has been a joint effort between ASU-PRL and Clean Energy Associates. This work carries out a statistical analysis of the results obtained through the above-mentioned pre-shipment evaluation by using the Failure Mode, Effect, and Criticality Analysis (FMECA) technique. First developed for the automobile industry, this method uses the Risk Priority Number (IEC 60812) which is a statistical tool to evaluate the standard of manufacturing for production facilities. Based on three defining criteria to evaluate the risk carried by an identified defect, this tool has quickly gained prominence across industries and has been suitably adapted to fit manufacturing standards for different products. This technique has been established in the field of photovoltaics by the Photovoltaic Reliability Laboratory at Arizona State University (ASU – PRL) in a prior

thesis [1]. The scope of this work is to suitably modify the RPN method for PV module manufacturing.

1.1.2 Statement of the Problem

The present system for evaluating the quality of manufacturing lacks in certain crucial assessments. Firstly, the assessment is limited to providing a percentage based on the number of defected modules observed through random sampling. It fails to account for the nature of the defect itself, and, more importantly, the effect it could have on the lifetime of the module. Hence, although performance evaluation is covered under flash testing, there remains a question over the long-term reliability of the modules being shipped. Secondly, the result of any quality assurance program should be a detailed analysis outlaying the risk being carried by the produced batch; a quantitative analysis which will enable comparisons with prior projects and scorecards for manufacturers. As the present method fails to provide detailed insight into the defects observed, it requires an upgrade to match up to quality control measures prevalent in other manufacturing industries. This thesis work outlines the methods involved in suitably adapting the FMECA approach to PV module manufacturing such that a benchmarking system is incorporated to enable comparisons among projects.

1.1.3 Objective

The main objectives of this study are as follows:

- Determine the failure modes at the time of manufacturing
- Define parameters to rank these failure modes on the criteria of severity, occurrence, and detectability
- Linearize the model to enable a comparative study
- Run the system for different projects to obtain an RPN for each project and set limits for manufacturing quality based on the scores obtained

1.2 LITERATURE REVIEW

1.2.1 FMEA/FMECA

Failure Modes and Effects Analysis (FMEA) is a qualitative method of reliability analysis (failure analysis) for any item, component, or system. This analysis is mainly done in Reliability, Safety and Quality Engineering and involves reviewing components, assemblies, and subsystems to identify failure modes, their causes and effects. During the design phase, the result of this analysis prioritizes the failures according to the consequences, occurrence, and detectability, thus drawing attention to eventual weaknesses in the system, in such a way as to reduce failures with necessary modifications and, more generally, improve reliability. [2] [3] [1]

FMECA extends FMEA with an addition of detailed quantitative analysis of criticality of failure modes. FMECA is a method to identify the potential failure modes of a product, process, device, or system manufactured with varying technologies (electrical, mechanical, hydraulic, etc.). FMEA/FMECA analysis allows a good understanding of the behavior of a component of a system, as it determines the effect of each failure mode and its causes. This assigns a rank to each of the failure modes according to their criticality, occurrence, and detectability. The study of criticality quantifies the effect of each failure mode, so that the effect of these failures could be minimized prior to action [3]

In the FMEA/FMECA analysis, the following procedures are followed[1], [3]:

- System Description: Defines the system, including its functional, operative, and environmental requirements.

- Definition of Failure Modes: The modes, the causes and the effects of failures, their relative importance, and their means of propagation are defined.
- Identifying the causes of failures: The causes of each failure mode are identified.
- Identifying the effects of failure modes: The effects of each failure mode in the system leading to different degradation or harm to environment or to the system are identified.
- Definition of measures and methods for identifying and isolating failures: Defines the ways and methods for identifying and isolating failures.
- Classification of the severity of final effects: The classification of the effects is carried out per the nature of the system under examination, the performance and functional characteristics of the system, especially regarding operator safety, and finally, guarantee requirements.

1.2.2 Risk Priority Number

This follows the IEC 60812 2006-01 Standard. First developed for the automobile industry, the Risk Priority Number is a statistical tool to evaluate the standard of manufacturing for production facilities. Based on three simple criteria to evaluate the overall risk carried by a project, this tool has quickly gained prominence across industries and has been suitably adapted to fit manufacturing standards for different products.

Risk Priority Number (RPN) works by ranking defects on 3 simple criteria, regardless of the product being analyzed, as illustrated below:

$$\mathrm{RPN} = \mathrm{S} \times \mathrm{O} \times \mathrm{D}$$

Where S: Severity – Measure of the impact, the failure will have on the lifetime of the product

O: Occurrence – The frequency of a failure over the sampling size

D: Detectability – The difficulty in spotting the failure

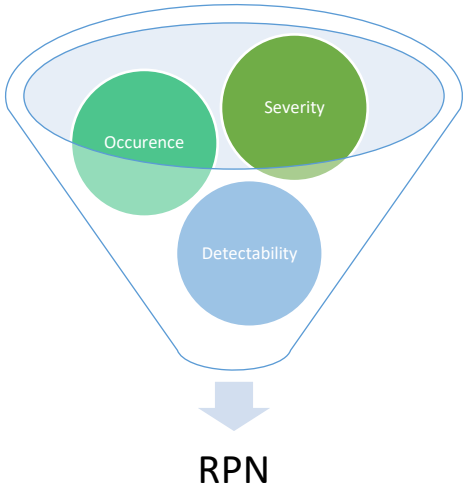

Figure 1.2-1 Components of Risk Priority Number

By this method, each failure is ranked from 1 – 10 on each of the above three criteria. The product of these ranks results in an RPN for each type of failure from the database being considered. Therefore, higher the RPN, higher the risk being carried by the project. The defect database will vary across industries. For PV module manufacturing, the defect database being implemented consists of 51 defects observed in PV modules at the time of production. This list has been developed by experienced professionals through analysis of over 3 GW of data of modules. It is to be noted that it is a subset of the entire list of defects observed in field aged modules as compiled by ASU-PRL in a prior thesis. [1]

Table 1.2-1, Table 1.2-2, and Table 1.2-3 below list the severity, occurrence, and detectability rankings as defined by the Standard.

Table 1.2-1 Determination of Severity

Severity	**IEC 60812 criteria**	**Rank**
None	No discernible effect	1
Very minor	Fit & finish/squeak and rattle do not conform. Defect noticed by discerning customers (less than 25%)	2
Minor	Fit & finish/squeak and rattle do not conform. Defect noticed by discerning customers (less than 50%)	3
Very low	Fit & finish/squeak and rattle do not conform. Defect noticed by discerning customers (less than 75%)	4
Low	Item operable but comfort/convenience item(s) operable at a reduced level of performance. Customer somewhat dissatisfied	5
Moderate	Item operable but comfort/convenience item(s) inoperable. Customer dissatisfied	6
High	Item operable but at a reduced level of performance. Customer very dissatisfied	7
Very high	Item inoperable (loss of primary function)	8
Hazardous with warning	Very high severity ranking when a potential failure mode affects safe operation and/or involves non-compliance with government regulation with a warning	9

Hazardous without warning	Very high severity ranking when a potential failure mode affects safe operation and/or involves non-compliance with government regulation without a warning	10

Table 1.2-2 Determination of Occurrence

Occurrence	**Cumulative Number of Defects (CND) (IEC 60812)**	**Rank**
Remote: Failure is unlikely	< 0.01 per thousand items	1
Low: Relatively few failures	< 0.1 per thousand items	2
	< 0.5 per thousand items	3
Moderate: Occasional failures	< 1 per thousand items	4
	< 2 per thousand items	5
	< 5 per thousand items	6
High: Repeated failures	< 10 per thousand items	7
	< 20 per thousand items	8
Very high: Failure almost inevitable	< 50 per thousand items	9
	>=100 per thousand items	10

Table 1.2-3 Determination of Detectability

Detection	**Criteria: Likelihood of detection by design control (IEC 60812)**	**Rank**
Almost certain	Design control will almost certainly detect a potential cause/mechanism and subsequent failure mode	1
Very high	Very high chance design control will detect a potential cause/mechanism and subsequent failure mode	2
High	High chance the design control will detect a potential cause/mechanism and subsequent failure mode	3
Moderately high	Moderately high chance the design control will detect a potential cause/mechanism and subsequent failure mode	4
Moderate	Moderate chance the design control will detect a potential cause/mechanism and subsequent failure mode	5
Low	Low chance the design control will detect a potential cause/mechanism and subsequent failure mode	6
Very low	Very low chance the design control will detect a potential cause/mechanism and subsequent failure mode	7

Remote	Remote chance the design control will detect a potential cause/mechanism and subsequent failure mode	8
Very remote	Very remote chance the design control will detect a potential cause/mechanism and subsequent failure mode	9
Absolutely certain	Design control will not and/or cannot detect a potential cause mechanism and subsequent failure mode; or there is no design control	10

The computed RPN, together with the level of severity, determines the critical failure mode, so that the focus could be concentrated to mitigate the effects from the failure. This means that, for failure modes with similar or identical RPN, the failure modes to be addressed first are those with the higher severity numbers. The failure modes are then ranked per their RPN, and high priority is assigned to high RPN. As we know from the above, the RPN is the product of S, O, and D, and the evaluation of RPN can present some problems such as [1], [3], [4]

- Gaps in the range: The RPN values are not continuous, but have only 120 unique values: 88% of the range is empty. Multiples of prime numbers greater than 7 do not feature in the list.

- Duplicate RPNs: Different values of the parameters may generate identical RPN values. The RPN numbers 60, 72, and 120 can each be formed from 24 different combinations of S, O, and D.
- High sensitivity to slight changes: Multiplying the numbers comprising the RPN is intended to magnify the effects of high risk factors. Thus, even a small variation in one of the parameters implies a notable variation in the RPN value.
- Inadequate scale of RPN: The difference in RPN value might appear negligible, whereas it is in fact significant. For example, the RPN1 with 3, 4, and 5 as S, O, and D, respectively, gives the value of 60, whereas the RPN2 with 3, 5, and 5 gives 75. In fact, in RPN2 the failure mode has the twice the occurrence, but the RPN value is not doubled. This explains that the RPN values cannot be compared linearly.

1.3 METHODOLOGY

The data acquired for this study was from the pre-shipment evaluations of modules in typical manufacturing facilities across the PV industry . Random lots were selected from the daily batches for inspection. Modules were visually inspected based on a pre-determined list of defects made available to the on-site engineers. Flash testing and EL imaging were performed at the manufacturing facility and the defect results were documented.

In his work on RPN for field aged modules, Shrestha ([1]) outlines the failure modes associated with modules aged in the field. On comparison with the defect list used in manufacturing quality inspection, it was ascertained that the failure modes being considered were, in effect, a subset of the larger set of failure modes seen in the field, as reported by ASU-PRL [1]. Failure modes such as discolored encapsulant, resistance values (series and shunt) outside accepted limits, and hotspots are not considered in this study. This is because, as the module manufacturing process has been standardized, certain failure modes arising from inferior quality manufacturing, as the ones described above, have been eliminated. Standardization of the manufacturing process has improved general internal quality control. Hence, failure modes such as low high shunt resistance, due to improper firing, or discolored encapsulant due to poor procurement, have been ironed out of the manufacturing process over time.

1.3.1 Determination of Severity

As defined earlier, Severity is a measure of the impact the defect has on the performance on the module. As with IEC 60812, the ranking system for PV modules has been designed with ascending order of severity - the greater the probable impact, the higher the rank.

For ranking, the list of defects was segregated into 4 types: Cosmetic, Minor, Major, & Critical. It is to be noted that, based on the severity, a defect can be minor, major, or critical. Each defect from the pre-defined list of defects was then categorized as per the 4 types based on the potential effect. The definitions for the categories are provided below in Table 1.3-1. Cosmetic defects have been defined as those which do not have a tangible impact on module performance. Examples include misaligned barcodes and extra sealant. However, such defects can point to a general carelessness in production and hence have been given a rank of 2. Minor defects are defined as those that have a minimal impact on performance and can be corrected. Defects such as small scratches on glass come under these defects. Minor defects have been split into 3 categories: Type 1, 2, 3 and hence defects falling under these categories are assigned severity ranks of 3, 4, and 5. Major defects are viewed as those having definitive impact on module performance. Defects such as delamination, cell mismatch and cell cracks come under this category. Like the category of Minor Defects, this category, too, is further sub divided into 3 types – 1, 2, 3 and defects falling in this category are assigned ranks of 6,7, and 8. The final category of defects is the Critical Defects. Complying with the Standard that defines the defect ranks, these defects are those which are not only certain to pose performance losses but also safety concerns and threat to life or property. Such defects are rarely observed at the end

of manufacturing lines as that would be represent a considerably bad manufacturer. Moreover, internal inspection ensures that such modules are replaced immediately and never make it to external quality inspection. Examples include broken glass and faulty wiring in the junction box. Based on a clear perceived threat to life or property, these defects are assigned ranks of 9 and 10 which are the highest ranks in this list.

Table 1.3-1 Categorization of defects

Cosmetic defects	Although it does not impact module reliability, the carelessness in having this defect indicates a general quality of production
	Rank: 2
	e.g.: Misaligned barcode
Minor defects	Have a minimal impact on reliability and can usually be corrected. Are subdivided into Type 1, 2, & 3
	Ranks: 3-5
	e.g.: Scratches on glass
Major defects	Can have a noticable impact on module reliability. Are subdivided into Type 1, 2, & 3
	Ranks: 6-8
	e.g.: Delamination
Critical defects	Will definitely have a negative impact on reliability and pose a threat to life
	Ranks: 9-10
	e.g.: Broken glass

As is the norm with quality assurance, the ranking system does include for cases where the modules are replaced altogether. Replaced modules are assigned rank 1. However, as the sampling sizes are usually 2-3% of the entire production orders, assigning this rank is statistically inaccurate as it is not representative of the entire production order. This rank

has been reserved for special cases when a more sizable portion of the orders is sampled. The ranking order, with a comparison to the original standard, has been provided in Table 3.1 below.

Table 1.3-2 Comparison of Severity ranks for PV module manufacturing with the Standard

Severity	**IEC 60812 criteria**	**PV module criteria**	**Rank**
None	No discernible effect	Replaced	1
Very minor	Fit & finish/squeak and rattle do not conform. Defect noticed by discerning customers (less than 25%)	Cosmetic defect	2
Minor	Fit & finish/squeak and rattle do not conform. Defect noticed by discerning customers (less than 50%)	Minor defect type 1	3
Very low	Fit & finish/squeak and rattle do not conform. Defect noticed by discerning customers (less than 75%)	Minor defect type 2	4
Low	Item operable but comfort/convenience item(s) operable at a reduced level of performance. Customer somewhat dissatisfied	Minor defect type 3	5

Moderate	Item operable but comfort/convenience item(s) inoperable. Customer dissatisfied	Major defect type 1	6
High	Item operable but at a reduced level of performance. Customer very dissatisfied	Major defect type 2	7
Very high	Item inoperable (loss of primary function)	Major defect type 3	8
Hazardous with warning	Very high severity ranking when a potential failure mode affects safe operation and/or involves non-compliance with government regulation with a warning	Critical defect without safety concerns	9
Hazardous without warning	Very high severity ranking when a potential failure mode affects safe operation and/or involves non-compliance with government regulation without a warning	Critical defect with safety concerns	10

1.3.2 Determination of Occurrence

The occurrence of the defect has been modelled as the "Cumulative Number of Defects", the formula for which as follows:

$$CND = \frac{No.\ of\ defects}{Total\ no.\ of\ modules} \times \frac{No.\ of\ lots\ passed}{Total\ no.\ of\ lots} \times 1000 \quad (1.3\text{-}1)$$

The CND accounts for the total no. of occurrences of each defect through the entire order. It also employs a correction factor for the lots passed by the third-party quality control firm. As with the case in severity, it would be advisable to include this correction factor only in cases where the lots being inspected are a high percentage, hereby ensuring that any failed lot does have an impact on the entire order. Lastly, to ensure a normalization, a multiplication factor of 1000 has been included – cumulative no. of defects per thousand modules. The calculated CND is subjected to the same ranking pattern as the standard, as seen in the Table 1.2-2.

1.3.3 Determination of Detectability

Kuitche et al [5] used an acceleration testing and qualification testing technique to determine the probability of detecting a failure mode. However, the FMECA analysis has outlined the field evaluation approach to be followed while assigning ranks for detectability. Based on this approach, the ranking is structured proportional to the ease of detection – the higher the chances of detectability, the lower the rank. In building the RPN system for PV Power Plant analysis, the ASU-PRL method defines ranks based on the likelihood of detection during field inspection. The lower ranks are reserved for

visually observable defects while the higher ranks are assigned based on the equipment used to spot the defect; defects spotted using conventional hand held tools used in the field (e.g. infrared camera) are assigned 4-6 while defects spotted using performance measuring equipment (e.g. I.V. curve tracer). Although this is perfectly applicable to field evaluations, translating this system to manufacturing evaluations required considerable review. This is because, while performance and durability measuring instruments such as I-V curve tracers are not readily available at a power plant site, flash testing and electroluminescence imaging systems are installed in-line in manufacturing facilities. Hence, detection of defects through these systems in manufacturing facilities is much easier than in field inspections. Therefore, detection ranks based on conventional and non-conventional instrument use is not applicable for manufacturing activity.

For the ranking order of detectability in manufacturing quality assurance, the idea was to focus directly on the general difficulty level in spotting defects during inspections. Subsequently, the defects were assigned ranks based on extensive prior experience of the teams in quality inspection projects. Each defect from the pre-determined list of defects had been assigned a rank between 1 and 10; higher the difficulty in spotting the defect, higher the rank. Hence, the ranking system for detectability remains the same as per the guideline in the Standard and has been detailed in Table 1.2-3.

1.3.4 Linearization of RPN

A major objective of this work has been to develop a method to allow for a quantitative comparison among projects. As outlined in section 1.1.2, at present, it is impossible for

clients and financers to have quantified assessments of projects in terms of manufacturing quality. Hence, it is vital that the RPN method developed takes steps in the direction of providing quality assessments of manufacturing which are easily comparable.

The FMECA approach providing the RPN is a product of 3 whole numbers. With this framework, the minimum rank for a defect can be 1 and the maximum can be 1000. However, since the RPN is a product of three numbers ranging from 1-10, numbers that cannot be expressed as products of such numbers i.e. prime numbers > 2, do not appear in the RPN list of numbers. As noted by Shreshtha in his thesis, there are only 120 unique values of RPN from 1-1000 which can feature for any defect [1]. As such, an inconsistent range does not suit well for rating and comparing projects hereby defeating the point of this work.

A suitable way to tackle this issue is by linearizing the RPN ranks by scaling them from 1 to 100. This is done by sequentially numbering the 120 RPNs and then dividing the sequence by 1.2, hereby obtaining a new scale which will be referred to as Ranked RPN.

In Figure 1.3-1 below, the plot summarizes the Linearization of RPN. On the x axis are the RPN values while the y axis contains the corresponding Ranked RPN values. The logarithmic nature of the graph is in close agreement with the general perception of risks associated with defects – beyond a critical RPN, the Ranked RPN will always be a high value, indicating an elevated risk.

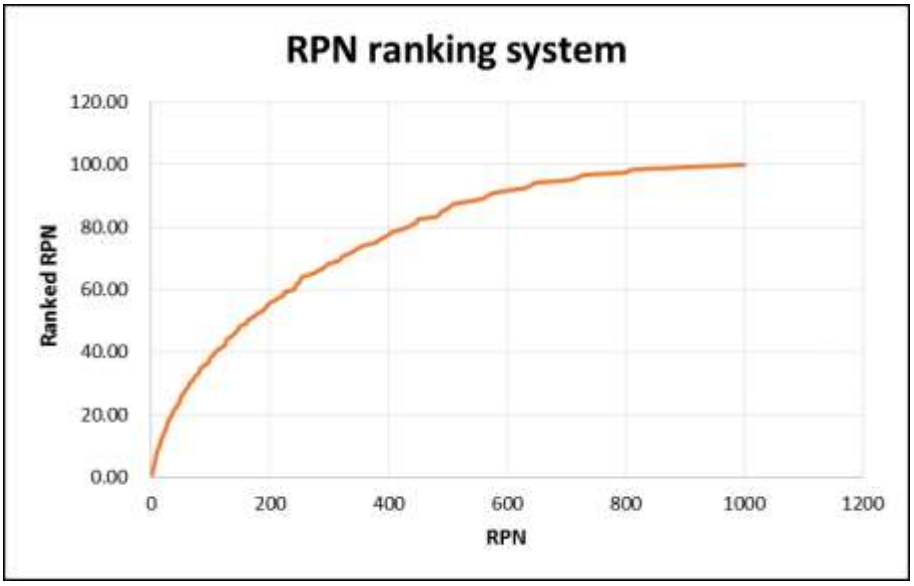

Figure 1.3-1 Linearization of RPN

1.3.5 Project Rank

Lastly, to arrive at one quantified risk assessment for the project, the individual Ranked RPNs of each defect are summed to provide a Project RPN. If linearization were not to be carried out, summing up the RPNs would result in an inconclusive result due to the gaps in the RPN range.

$$Project\ RPN\ = \sum_{i=1}^{3} Avg\ of\ linearized\ RPN\ of\ major\ type\ i + \sum_{i=1}^{2} Avg\ of\ linearized\ RPN\ of\ critical\ type\ i \quad (1.3\text{-}2)$$

As can be seen in $Project\ RPN\ = \sum_{i=1}^{3} Avg\ of\ linearized\ RPN\ of\ major\ type\ i + \sum_{i=1}^{2} Avg\ of\ linearized\ RPN\ of\ critical\ type\ i$ .. (113-2), the Project RPN is the aggregate of the Ranked RPNs of the individual major and critical defects. The two defect types that have been excluded are the cosmetic defects and the minor

defects and the reason for this is in the way these two categories were defined. Cosmetic defects are defined as those with no impact on module performance and minor defects are those with minimal impact on module performance and reliability. Hence, minor and cosmetic defects are not included in Project RPN as they do not largely impact module reliability and bankability.

1.4 RESULTS AND DISCUSSION

This chapter deals with the implementation of the modified FMECA technique to calculate Ranked RPN values for PV module manufacturing projects. The assessments have been conducted based on the in-line visual inspection, electroluminescence imaging, and flash testing reports of certain projects. The Ranked RPN technique will be applied to three projects (project 1, project 2, and project 3) and the results will be analyzed. Each module received and RPN and, subsequently, each project received an RPN, which allows for a quantitative comparison system. To remain manufacturer and module blind, the manufacturer, the facility, and the module type will not be revealed.

1.4.1 Ranked RPN for project 1

Let us consider the project detailed in Table 1.4-1 wherein nearly 6000 modules were inspected at random as per a pre-decided sampling rate through the quality assurance program. With the prevalent system, a defect rate of 5% had been reported which fails to provide insight into the nature of defects and the gravity of the risk.

Table 1.4-1 Project 1 information

Project Information	
Number of modules	5598
Defect rate	5%
Module construction	Glass-encapsulant-cell-backsheet

The modified FMECA approach has been incorporated to analyze this project. Pre-shipment evaluations (visual defects and electroluminescence imaging) revealed the defects that were identified in the modules. Each defect was then ranked based on severity, occurrence, and defect. The product of these ranks resulted in an RPN for each defect. The list of defects observed and their corresponding ranked RPNs have been detailed in Table 1.4-2 :

Table 1.4-2 Defect analysis for Project 1 through RPN

Category	**Defect**	**RPN**	**Ranked RPN**
Cell	Cracked corner & cell chip	84	35
	Cell scratches	24	15
	Cell contamination from non-module components	90	36
	EVA bubble/residue	224	58
	Cell contamination from module components	120	42
	Considerable cell color difference	40	22
Cell String	Cell to cell spacing	140	46
	Cell to edge spacing	150	48
	Cell to collection ribbon spacing	56	28
	Ribbon alignment	126	43
Glass	Contaminations (finger prints, stains, residual encapsulant) on glass	48	24

	Scratch on glass	60	28
Backsheet	Backsheet contaminations	60	28
	Scratches on backsheet foil	120	42
	Dents on backsheet foil	90	36
	Elevated soldering points	50	26
	Bubbled/voids, wrinkles, holes on backsheet foil	96	37
Frame	Frame surface defect (scratches, corrosion, dent, blister)	72	32
	Frame assembly gap in the corner	8	7
	Frame assembly roughness (corner edge)	16	12
	Insufficient/Excessive sealant	48	24
Junction Box	Junction box alignment	8	7
	Insufficient/excessive sealant	140	46
Final Assembly	Unreadable/unclear bar code	8	7
Other	Other	120	42
EL	Broken cells	64	30
	Micro cracks	196	55
	Tree shape micro cracks	144	47
	Cell class difference	18	15

A better understanding of the distribution of the defects is presented in Figure 1.4-1 below. It shows the distribution of the Ranked RPNs across the severity types. The even spread of the Ranked RPNs suggests no special cause variation i.e. there are many common causes inherent in the process which are leading to an even spread of defects. In this case, it is suggesting that minor and major types of defects are, both, equally prevalent, with moderate average values of Ranked RPNs, considering the highest possible is 120. It is expected to not have critical defects at this stage, due to a combination of an optimized manufacturing process and improvements in internal quality control. Among the major defects, reliability concerns arising from cell level micro cracks and imperfect encapsulant lamination require mitigating efforts.

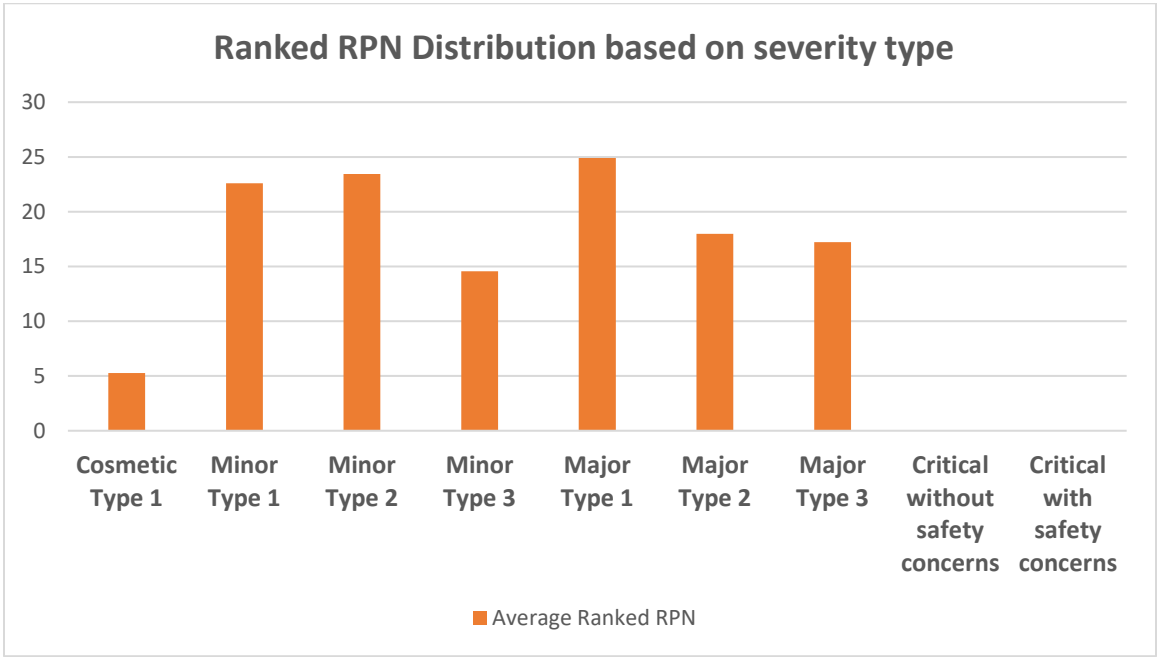

Figure 1.4-1 Ranked RPN distribution based on severity type

The Ranked RPN for this project is 60, which is a significantly high number when compared with the present internal benchmarks. It implies that the project carries significant risk in terms of the reliability of the modules, a conclusion which was not captured in the 5% reported defect rate.

1.4.2 Ranked RPN for project 2

The second project, detailed in Table 1.4-3 selected for analysis was a quality inspection conducted in a different facility. The number of modules inspected, based on a pre-defined sampling rate, were 13813 from different batches. In this case, the defect rate reported was close to 0%, suggesting minimal reliability concerns.

Table 1.4-3 Project 2 information

Project Information	
Number of modules	13813
Defect rate	0%
Module construction	Glass-encapsulant-cell-backsheet

The pre-shipment evaluations threw up the nature of the defects observed. Each defect was ranked as per the FMECA process to result in an overall Ranked RPN for the project. The list of defects observed, and their corresponding RPNs, is listed in

Table 1.4-4 :

Table 1.4-4 Defect analysis for Project 2 through RPN

Category	Defect	RPN	Ranked RPN
Cell	Cell scratches	64	30
	Cell contamination from non-module components	42	23
	Cell contamination from module components	60	28
Cell string	Cell to cell spacing	48	24
	Cell to collection ribbon spacing	84	35
	Ribbon alignment	96	37
Glass	Scratch on glass	24	15
Frame	Frame surface defect (scratches, corrosion, dent, blister)	36	21
	Frame assembly gap in the corner	12	9
	Insufficient/Excessive sealant	70	31
Junction box	Junction box alignment	8	7
	Insufficient/excessive sealant	105	39
Other	Other	30	18
EL	EL micro cracks	84	35

The plot below is the distribution of the average Ranked RPN based on the severity type. As was the case with project 1 analysis, the Ranked RPNs are distributed evenly across all the severity types, indicating that the manufacturing process is adequate in quality control. However, in comparison with the previous project, the magnitudes are much lesser, indicating much lesser risk. Among the major defects, cell contamination and ribbon alignment were ascertained as failure modes which could lead to moderate reliability issues. As expected, no critical defects were observed.

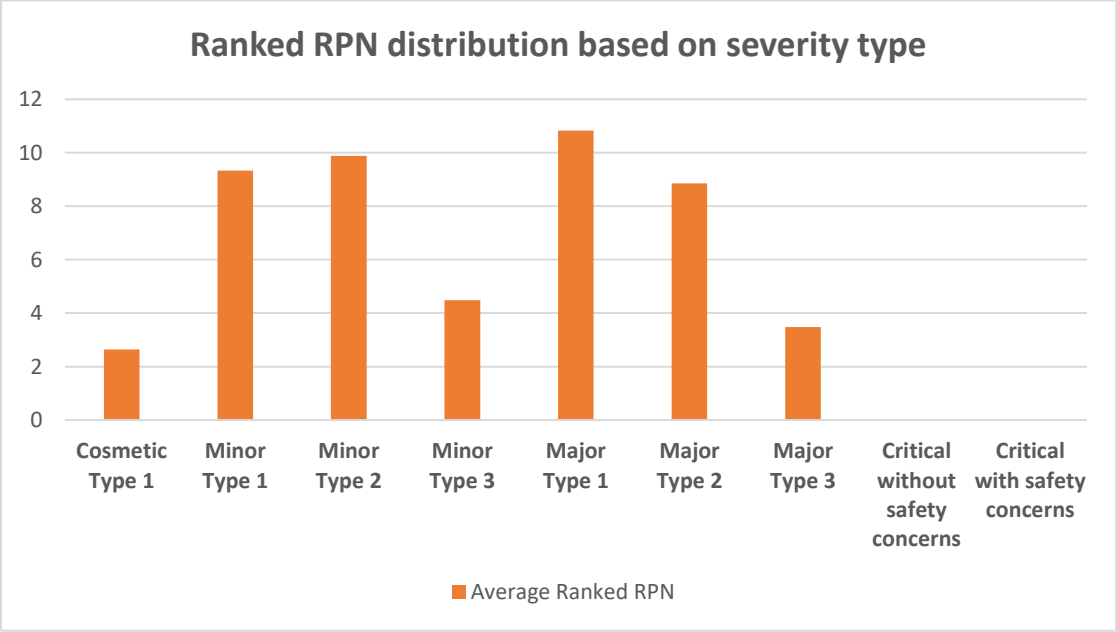

Figure 1.4-2 Ranked RPN distribution based on severity type for Project 2

The overall project Ranked RPN, based on the Ranked RPNs of the major and critical defects, was calculated to be 23. Comparing with the internally developed benchmarks,

this suggested that the project carried minimal risk in terms of module bankability, which agreed with the conclusion drawn from the defect rate analysis.

1.4.3 Ranked RPN for project 3

The final analysis using the modified FMECA approach is for project 3, detailed in Table 1.4-5, wherein near 6000 modules were inspected as per the preset sampling rate. The defect rate reported for this project was 2%, suggesting minimal module reliability concerns.

Table 1.4-5 Project 3 information

Project Information	
Number of modules	5893
Defect rate	2%
Module construction	Glass-encapsulant-cell-backsheet

Based on the pre-shipment evaluations, the defects observed through visual inspections and EL imaging were ranked for severity, occurrence, and detectability to yield corresponding RPN values. The analysis for the defects is presented in Table 1.4-6:

Table 1.4-6 Defect analysis for Project 3 through RPN

Category	**Defect**	**RPN**	**Ranked RPN**
Cell	Cracked cell	42	23
	Cracked corner & cell chip	60	28

	Cell scratches	96	37
	Cell contamination from non-module components	105	39
	EVA bubble/residue	112	41
	Cell contamination from module components	48	24
Cell string	Cell to cell spacing	60	28
	Cell to edge spacing	40	22
	Cell to collection ribbon spacing	48	24
	Ribbon alignment	45	23
Glass	Inclusions, bubbles on glass	80	33
	Scratch on glass	50	26
Backsheet	Backsheet contaminations	36	21
	Scratches on backsheet foil	48	24
	Dents on backsheet foil	42	23
Frame	Frame surface defect	60	28
	Frame assembly gap in the corner	16	12
	Insufficient/Excessive sealant	50	26
Junction box	Insufficient/excessive sealant	100	38
Final assembly	Label alignment/label smear/label damaged	8	7
Other	Other	150	48

EL	Micro cracks	120	42
	Tree shape micro cracks	96	37

The distribution of the average Ranked RPN is illustrated in Figure 1.4-3. The even spread of the average Ranked RPNs suggested common cause variation with no specific fault in the manufacturing process. The minor defects seem to be slightly higher than the major defects. However, there are certain major defects, such as micro cracks, which do raise medium concerns on the long-term reliability of the modules.

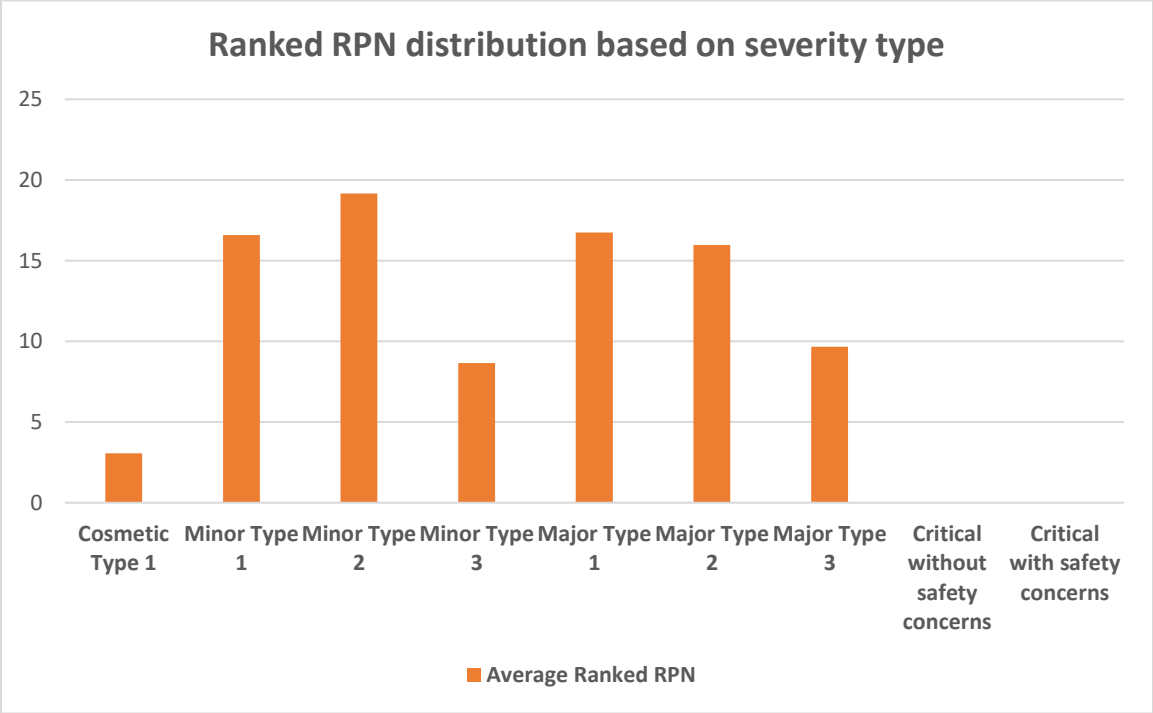

Figure 1.4-3 Ranked RPN distribution based on severity type for Project 3

The Ranked project RPN is calculated to be 47. It indicates a medium level of risk being carried by the project in terms of module reliability. Cell level concerns, although not

critical, have raised the overall Ranked RPN for this project, a factor not captured in the 2% reported defect rate.

1.4.4 Scope for improvement

There remains scope for improvement in the FMECA system for PV module manufacturing. At present, the severity and detectability ranks have been assigned based on prior experience, leading to a subjective evaluation. One recommendation would be to have a more objective system of ranking, thereby eliminating human error. ASU-PRL have devised a severity ranking system based on the power degradation of the module. Attempts were made to translate this to manufacturing but in vain. This is because, the flash tests conducted during quality control revealed negligible differences in current voltage parameters in comparison with those reported by the manufacturers. As such, having a ranking system based on this difference would be implausible.

One possible solution would be to have a severity ranking system based on the electroluminescence imaging of the modules subjected to quality control. These ranks would be based on the ratio of light areas to the dark areas of the module or, in other words, the ratio of the regions of the module emitting light to those not emitting light under the forward bias conditions of this test.

1.5 CONCLUSION

By applying statistical techniques for quality control, the FMECA approach for PV module manufacturing can be a step in improving the bankability of modules. As each defect is systematically ranked on three criteria, the score of each defect can immediately inform the client about the nature of the defect and the overall risk posed by it on the project. This can enhance risk mitigation and measures to safeguard against any possible effects from these defects. Moreover, clients will also benefit from an overall quantified risk assessment for the project and be in a better position to judge project value.

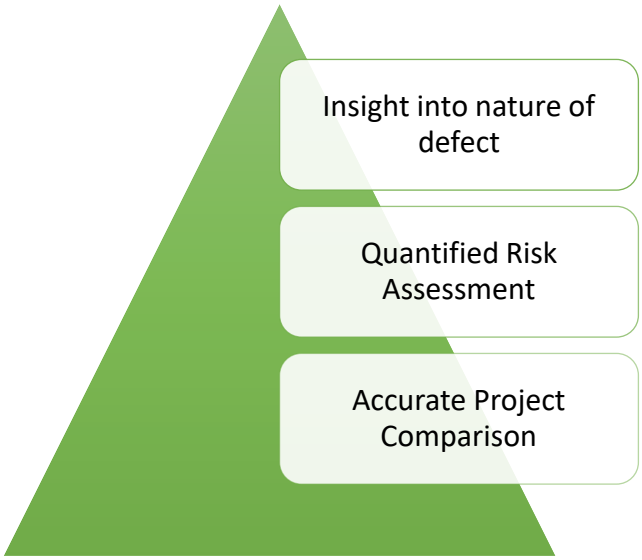

A standardized criterion for quality assurance in PV module manufacturing will also open the door for accurate project comparisons across the board. With the analysis of more projects through the RPN tool, a ready database will be generated which can allow for

ascertaining Ranked RPN benchmarks for quality standards (e.g. high risk, medium risk, low risk). Such a system can lead to scorecards for every manufacturer, as have been generated through the database at present, which will help clients make more informed decisions.

PART 2: CLIMATE DEPENDENT RELIABILITY - ACTIVATION ENERGY DETERMINATION FOR CLIMATE SPECIFIC DEGRADATION MODES

2.1 INTRODUCTION

2.1.1 Background

Photovoltaic modules operating in the field can experience diverse types of failure modes, based on three governing factors – the climatic conditions, the electrical configurations, and the manufacturing quality. This part of the thesis focusses on the failure modes associated with the climatic conditions the module is exposed to. Different climatic degradation modes, such as solder bond degradation, or corrosion, can impact the power output of the module to a different degree. It is important to understand the impact of each climatic degradation mode to make improvements in the reliability of modules in these climates.

This work attempts to model the influence of specific climatic degradation modes on the long- term reliability of modules. The analysis has been conducted by modelling the time to failures for modules as functions of a combination of climatic conditions i.e. temperature, relative humidity, and ultraviolet radiation. The module time to failure data for this analysis was sourced from accelerated tests conducted at ASU-PTL and field data obtained through field evaluations conducted by ASU-PRL, amounting to nearly a 1000 modules. The weather data was obtained through the Typical Meteorological Data files available on the NREL website [6]. After analyzing models, the best fit was tested by comparing the activation energies obtained for individual degradation modes with those reported in literature.

2.1.2 Statement of the problem

The present system to model the impact of individual climatic degradation mode is based on the power degradation of the module. Numerous climatic degradation modes can affect the power output of the module. Hence, this method of analysis may inaccurately estimate the impact of one degradation mode on the overall power output of the module or, in other words, this method may inaccurately associate the influence of one degradation mode with another since the power output values do not differentiate between the different climatic degradation modes. Hence, it is important to develop predictive models based on the performance parameter directly influenced by the degradation mode under investigation. This thesis work attempts to understand the pathways for climatic degradation modes, the performance parameters they impact, and develop a model to associate the climatic conditions at the site with the relevant performance parameter degradation.

2.1.3 Objectives

The main objectives of this study are as follows:

- Identify the performance parameter directly influenced by the degradation mode
- Develop a predictive model and define the constants
- Obtain the activation energy for different degradation modes as a way to validate the approach
- Test for different climatic conditions

2.2 LITERATURE REVIEW

2.2.1 Climate based degradation modes

The power degradation in PV modules can be due to numerous failure modes that build within the module over time. A comprehensive list of failure modes has been listed by M. Moorthy in his work on Risk Priority Numbers for failure modes in field aged modules.[7]. The 86 defects listed can be split into defects which may have occurred due to a fault in manufacturing and defects that have built up over time due to climate stresses. M. Chicca analyzed Siemens M55 modules recovered from different climate zones. The results indicated that the degradation was significantly based on the climate type, with the IV parameter most affected differing based on the climate the module was in; there was significant short circuit current degradation in the modules fielded in Arizona and California while fill factor degradation seemed to dominate in Colorado. [8]

The section hereafter attempts to relate climate-based degradation modes with the primary parameters that govern the power output of the module i.e. Isc, Voc, and FF.

2.2.2 Identifying pathways for short circuit current degradation

Pern et al. have investigated the browning mechanism and its effect on Isc. [9]. A combination of ultraviolet light and temperature is known to cause a degradation reaction of the encapsulant (EVA), which results in chromophore formation and subsequent browning of the encapsulant. This discoloration directly affects the current generation capability of the solar cells, as it limits the number of photons hitting the cells, in turn reducing the short circuit current of each cell.

Delamination, on the other hand, is the optical decoupling of the encapsulant with the solar cell or with the glass on top. This adhesion between the glass, encapsulant, active layers, and back layers can be compromised for many reasons. Typically, if the adhesion is compromised because of contamination (e.g. improper cleaning of the glass) or environmental factors, delamination will occur, followed by moisture ingress and corrosion. This results in an airgap, either between the glass and encapsulant or between the encapsulant and the cell, or both, which further refracts the incoming light and reduces the current generating capacity of the cell [10].

2.2.3 Identifying pathways for open circuit voltage degradation

The voltage generating capacity of the cell is directly proportional to the bandwidth of the material utilized in manufacturing the cell. It can be affected at the time of manufacturing, such as due to incorrect firing techniques. As the bandwidth is unaffected by weather conditions, Voc degradation is minimal over the lifetime of the module, as evidenced by field investigations cited in multiple field evaluation reports prepared by ASU-PRL.

Potential induced degradation is one major degradation mode based on climate and electrical configuration that can affect the open circuit voltage., largely affecting regions in the strings with a distinct voltage polarity with the ground. The effect can be understood as the migration of ions from the front glass through the encapsulant to the anti-reflective coating (SiNx) at the cell surface [11] driven by the leakage current in the cell to ground circuit. This leakage current is typically in the order of μA and its value is

strongly depending on material properties, the surface conditions, and humidity, as well as module temperature and the applied voltage. [10]

2.2.4 Identifying climate pathways for Fill Factor degradation

Fill factor of the module is affected by a degradation of the intermetallic system i.e. degradation of the gridlines, bus bars, interconnects and other metallic components in the electrical circuit within the module. The IMS degradation can be identified through an increase in the resistance values obtained. It has been noted that series resistance is the dominant resistance increase. Shunt resistance remains largely unaffected by weather conditions as it is a parameter fixed at the time of manufacturing.

Series resistance, on the other hand, can be affected by solder bond degradation. One form of this degradation is a mechanical degradation due to thermal stresses accrued over time. In his work, Dr. Bosco attempted to model solder bond degradation due to thermal stresses, known as thermal fatigue, using the Coffin Manson equation; the activation energy reported for this degradation mode was 0.12eV [12]. Another pathway for solder bond degradation occurs due to the formation of intermetallic compounds (IMC) which reduce the conductivity between the ribbons and the bus bars. The formation of IMC's is dependent on the composition of the solder bond, whether it contains lead, and the ratios of the other components. Geipel et al. modelled the growth of IMC's in solar interconnects by thermally aging prepared samples and analyzing the results through spectroscopy techniques. They reported activation energies for the growth of different IMC's in the solder bonds based on the composition, ranging from 0.8 – 1.5 eV[13].

2.2.5 Acceleration factor modelling

So far, models relating time to failure in accelerated testing environments to time to failure in field conditions have been based on power degradation of the modules. Kimball et al modelled the time to failures observed in DH1000 to arrive at the following expression for a corrosion based degradation mechanism[14]:

$$Time\ to\ failure\ (ttf)\ in\ condition\ i = \frac{1}{\frac{\partial \sigma}{\partial t}(T, RH)\ in\ condition\ i} \qquad (2.2\text{-}1)$$

Where: $\frac{\partial \sigma}{\partial t}(\mathrm{T}, \mathrm{RH}) = \mathrm{A} \exp\left(\frac{-\mathrm{Ea}}{\mathrm{kT}}\right) \mathrm{RH}^{\mathrm{n}}$

The activation energy reported for the corrosion reaction in this work was 0.79eV.

Moreover, he defined an acceleration factor to extrapolate the results of DH1000 testing to modules installed in the field based on the climate type:

$$Acceleration\ Factor = \frac{\frac{\partial \sigma}{\partial t}(T, RH)\ in\ accelerated\ test}{\frac{\partial \sigma}{\partial t}(T, RH)\ in\ field\ test} \qquad (2.2\text{-}2)$$

Similarly, Koehl modelled an acceleration factor between DH1000 and field conditions based on the climate type in an Arrhenius equation as the following: [15]:

$\mathrm{a}(\mathrm{T}_1, \mathrm{T}_2) = \exp(\frac{\mathrm{Ea}}{\mathrm{R}}\left(\frac{1}{\mathrm{T}_1} - \frac{1}{\mathrm{T}_2}\right)$; where the activation energy for the degradation mode associated with Damp Heat testing varies from 0.2 – 0.9 eV based on the testing time and the climate type.

2.3 METHODOLOGY

The analysis to calculate activation energies for different degradation modes has been conducted with data available at ASU – PRL. The accelerated testing data for DH1000 was recovered from the ASU-PTL archives. The data for field aged modules was obtained from field evaluations conducted by ASU-PRL.

2.3.1 Isolation of parameter based on degradation mode

PV modules are subjected to different climate related degradation modes in the field. M. Moorthy [7] has listed all the failure modes seen in the field. Some of the common degradation modes observed include encapsulant browning, solder bond degradation, and corrosion. As discussed in section 2.1, predictive models assessing the impact of these degradation modes are based on Pmax degradation. However, extensive field analysis has indicated that individual IV parameters i.e. Isc, Voc, FF are affected to different degrees based on the degradation mode.

Specific degradation modes influence certain IV parameters; using Pmax drop values to ascertain the impact of one degradation mode may be inaccurate as the Pmax could possibly be affected to a higher extent due to another degradation mode.

A better approach to predictive models for specific degradation models could be by delving one step deeper.

Pmax is defined as: $\mathrm{Pmax} = \mathrm{Isc} \times \mathrm{Voc} \times \mathrm{FF}$

As Pmax is a product of 3 parameters, the Pmax degradation should be proportional to the individual degradations of the three factors respectively. This hypothesis, supplemented by the literature surveys cited in section 2.2.1, leads us to a climate-based degradation pathway as described in Figure 2.3-1 below.

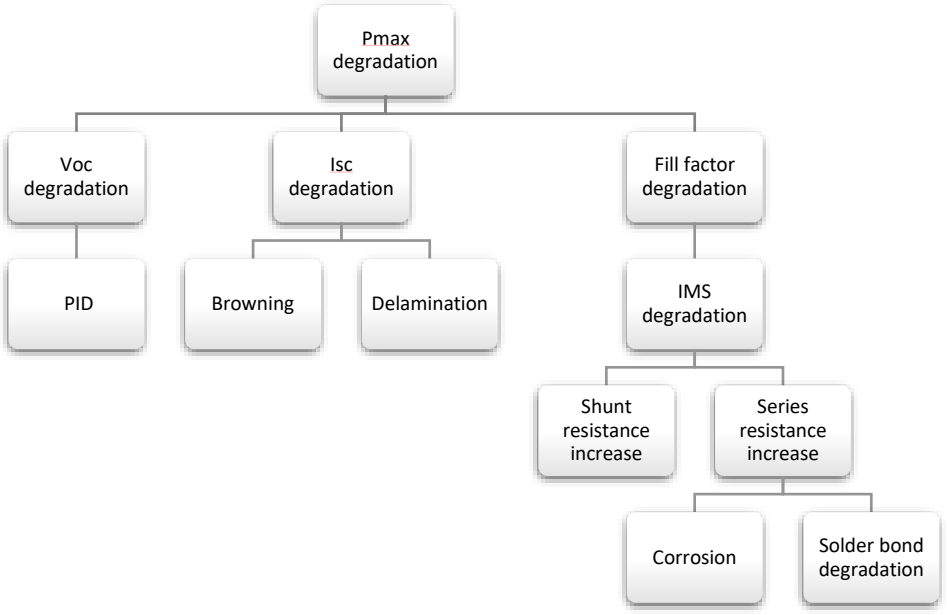

Figure 2.3-1 Pathways for climatic degradation modes

The degradation pathways give a clearer picture of the effect of each degradation mode. open circuit voltage is primarily degraded due to PID effects, which involve a combination of voltage polarity and climate conditions. The short circuit current of the modules is affected due to encapsulant degradation and delamination. The fill factor is affected due to IMS degradation. IMS degradation can be due to shunt resistance or series resistance increase. Hence, depending on the degradation mode being analyzed, the appropriate performance parameter directly affected should be assessed.

It has been noted that encapsulant degradation and IMS degradation are the two primary climate-based degradation modes, and hence are the two degradation modes that are being considered in this work. The table below summarizes the IV parameter that was focused on based on the degradation mode being considered:

Table 2-1 Identifying the performance parameter for degradation modes under investigation

Degradation mode	IV parameter
IMS degradation	Series resistance (Rs)
Encapsulant degradation	Short circuit current (Isc)

2.3.2 Model development

The basis for calculating activation energy for each degradation mode is by comparing the time to failure of the module at two different temperatures i.e. an acceleration factor which can be subsequently modelled based on the climate conditions.

Hence, the acceleration factor can be defined in two ways – 1) the ratio of the time to failure in the field test to the time to failure in the accelerated test 2) the ratio of the stress rate in the accelerated test to the field conditions.

As defined by Kimball et al [14] , time-to-failure (ttf) and stress rate have an inverse relationship:

$$Time\ to\ failure\ (ttf)\ in\ condition\ i = \frac{1}{\frac{\partial \sigma}{\partial t}(T,RH)\ in\ condition\ i} \quad (2.3\text{-}1)$$

Where: $\frac{\partial \sigma}{\partial t}(\mathrm{T}, \mathrm{RH}) = \mathrm{A} \exp\left(\frac{-\mathrm{Ea}}{\mathrm{kT}}\right) \mathrm{RH}^{\mathrm{n}}$

Therefore:

$$\frac{Time\ to\ failure\ (ttf)\ in\ field\ test}{Time\ to\ failure\ (ttf)\ in\ accelerated\ test} = Acceleration\ Factor = \frac{\frac{\partial \sigma}{\partial t}(T, RH)\ in\ accelerated\ test}{\frac{\partial \sigma}{\partial t}(T, RH)\ in\ field\ test} \quad (2.3\text{-}2)$$

Consider the left-hand side of equation 2.3-2:

$$\frac{ttf_{field}}{ttf_{accelerated}} = AF \quad (2.3\text{-}3)$$

Time to failure is dependent on the pre-determined limit or threshold beyond which the module is considered to have failed. Substituting into the equation:

$$\frac{threshold \times \frac{age_{field}}{degradation_{field}}}{threshold \times \frac{age_{accelerated}}{degradation_{accelerated}}} = AF \quad (2.3\text{-}4)$$

$$\frac{\frac{degradation_{accelerated}}{age_{accelerated}}}{\frac{degradation_{field}}{age_{field}}} = AF \quad (2.3\text{-}5)$$

Solving the above equation leads to:

$$\frac{Rd_{accelerated}}{Rd_{field}} = AF \tag{2.3-6}$$

The acceleration factor can, hence, be defined as the ratio of the rates of degradation of the modules in accelerated testing to field testing respectively.

Let us now consider the right-hand side of Equation 2.3-2.

$$Acceleration\ Factor = \frac{\frac{\partial \sigma}{\partial t}(T, RH)\ in\ accelerated\ test}{\frac{\partial \sigma}{\partial t}(T, RH)\ in\ field\ test} \tag{2.3-7}$$

The stress rate is defined using Peck's equation:

$$Stress\ rate:\ \ \frac{\partial \sigma}{\partial t}(T, RH) = A\ exp\left(\frac{-Ea}{kT}\right) RH^n \tag{2.3-8}$$

Substituting Equation 2.3-8 in 2.3-7 yields:

$$AF = \frac{exp\left(\frac{-Ea}{kT_{acc}}\right) {RH_{acc}}^n}{exp\left(\frac{-Ea}{kT_{field}}\right) {RH_{field}}^n} \tag{2.3-9}$$

Solving Equation 2.3-9 and equating with 2.3-6 results in:

$$\frac{Rd_{Acc}}{Rd_{field}} = AF = exp\left(\frac{-Ea}{k}\left(\frac{1}{T_{Acc}} - \frac{1}{T_{field}}\right)\right)\left(\frac{RH_{Acc}}{RH_{field}}\right)^n \tag{2.3-10}$$

2.3.3 Selecting models for degradation mode

2.3.3.1 Inter metallic system degradation

Two types of analysis were considered for IMS degradation:

1. Accelerated testing degradation to field degradation (A2F): Acceleration factor is defined as the ratio of the rate of degradation in accelerated testing (DH1000) to the rate of degradation in the field

2. Field 1 degradation to field 2 degradation (F2F): Acceleration factor is defined as the ratio of the rate of degradation in one field of a climate type to the rate of degradation of another field in another climate type

For both the above types of analysis, two models were considered: 1) the Arrhenius equation and 2) the Pecks equation (as developed in the previous section), both of which have been defined below. As discussed in 2.3.1, the IV parameter directly affected by IMS degradation is series resistance. The series resistance was calculated by the Dobos method [16]:

$$Rs = 0.34 \times \frac{V_{oc} - V_{mp}}{I_{sc}} \tag{2.3-11}$$

The calculation models used were defined as:

Arrhenius equation: $\frac{Rs\ increase\ rate_{Acc}}{Rs\ increase\ rate_{field}} = AF = exp\left(\frac{-Ea}{k}\left(\frac{1}{T_{Acc}} - \frac{1}{T_{NY}}\right)\right)$ (2.3-12)

Pecks equation: $\frac{Rs\ increase\ rate_{Acc}}{Rs\ increase\ rate_{field}} = AF = exp\left(\frac{-Ea}{k}\left(\frac{1}{T_{Acc}} - \frac{1}{T_{NY}}\right)\right)\left(\frac{RH_{Acc}}{RH_{NY}}\right)^{n}$ (2.3-13)

The difference between the two models is the consideration of relative humidity in the Pecks equation.

2.3.3.2 Encapsulant degradation

The type of analysis conducted for encapsulant degradation was:

1. Field 1 degradation to field 2 degradation (F2F): Acceleration factor is defined as the ratio of the rate of degradation in one field of a climate type to the rate of degradation of another field in another climate type.

In the case of encapsulant degradation, one of the main climate factors is the exposure to ultraviolet radiation. So far, the IEC 61215 does not prescribe an accelerated testing sequence involving ultraviolet light that is long enough to initiate discoloration of the encapsulant. Hence, A2F is not possible due to lack of accelerated testing data. Instead, field data from Arizona was considered as accelerated testing data due to the high UV dosage all year round there.

As discussed in the earlier section, the IV parameter considered is the short circuit current drop (Isc).

Three models were considered for data fitting for encapsulant degradation:

Arrhenius equation: $\frac{Isc\ degradation_{AZ}}{Isc\ degradation_{field}} = AF = exp\left(\frac{-Ea}{k}\left(\frac{1}{T_{AZ}} - \frac{1}{T_{field}}\right)\right)$ (2.3-14)

Modified Arrhenius equation:

$$\frac{Isc\ degradation_{AZ}}{Isc\ degradation_{field}} = AF = exp\left(\frac{-Ea}{k}\left(\frac{1}{T_{AZ}} - \frac{1}{T_{field}}\right)\right)\left(\frac{UV_{AZ}}{UV_{field}}\right)^{m} \quad (2.3\text{-}15)$$

Modified Pecks equation:

$$\frac{Isc\ degradation_{AZ}}{Isc\ degradation_{field}} = AF = exp\left(\frac{-Ea}{k}\left(\frac{1}{T_{AZ}} - \frac{1}{T_{field}}\right)\right)\left(\frac{RH_{AZ}}{RH_{field}}\right)^{n}\left(\frac{UV_{AZ}}{UV_{field}}\right)^{m} \quad (2.3\text{-}16)$$

The three models allowed to investigate the effect of climate factors on encapsulant discoloration. The Arrhenius model checks for the discoloration dependence on solely temperature. The modified Arrhenius equation includes a term accounting for the UV dosage in the field in comparison with Arizona. The modified Pecks equation considers the impact of temperature, UV, and relative humidity in combination on encapsulant degradation.

2.3.4 Model application

This section deals with the application of the model developed above in obtaining activation energies for each degradation mode. Let us consider the modified Pecks equation, as it includes all the climate factors being investigated:

$$\frac{Isc\ degradation\ rate_{AZ}}{Isc\ degradation\ rate_{field}} = AF = exp\left(\frac{-Ea}{k}\left(\frac{1}{T_{AZ}} - \frac{1}{T_{field}}\right)\right)\left(\frac{RH_{AZ}}{RH_{field}}\right)^{n}\left(\frac{UV_{AZ}}{UV_{field}}\right)^{m} \quad (2.3\text{-}17)$$

2.3.4.1 Degradation rates:

The Isc degradation rates (%/year) can be obtained from the information in the database. The ratio of these values will result in the AF.

2.3.4.2 Module temperature:

The Sandia model was utilized to obtain module temperature:

$$T_{module} = E.exp\big(a + b.(WS)\big) + T_{ambient} \quad (2.3\text{-}18)$$

Where: E: Plane of array irradiance

WS: Wind speed

Constants: a = -3.56, b = -0.075

The ambient temperature and wind speed were obtained from the TMY files available online. Care was taken to select temperature data from a weather station as close as possible to the actual site where the modules were installed. The plane of array irradiance

was calculated from the direct normal irradiance data in the TMY files through a tool sourced from Dr. Kempe at the National Renewable Energy Laboratory, Colorado. Hence, the module temperature was obtained on an hourly basis.

2.3.4.3 Ultraviolet light:

The ultraviolet dosage for any region is assumed to be 5% of the plane of array irradiance obtained from the TMY data.

2.3.4.4 Relative Humidity:

The module relative humidity was calculated using the same tool used for calculating plane of array irradiance. The ambient humidity was obtained from TMY files, recorded on an hourly basis. However, the tool is limited due to certain factors. Firstly, the choice of backsheet material determines the moisture diffusion and oxygen diffusion through to the cell. Secondly, the values obtained through the tool indicated relative humidity values higher than 100% within the module. This case was observed in New York when temperatures were less than -15^{o}C. Although this is possible in cases of super saturation, as air pressure is not likely to exceed atmospheric pressure within the module, the tool seems to lack in accounting for sub-zero temperatures. Hence, model calculations were done using module humidity and ambient humidity.

2.3.4.5 Calculation of the activation energy

The final activation energy is obtained through reverse calculations. Encapsulant degradation is known to occur from a set of reactions occurring within the encapsulant based on the conditions. However, for one climate, it is plausible to assume that one reaction pathway will be the dominant mode. Hence, encapsulant of the same general composition should have the same reaction pathway i.e. same activation energy in one climate.

The acceleration factor is obtained through the ratio of the performance parameters:

$$\frac{Isc\ degradation\ rate_{AZ}}{Isc\ degradation\ rate_{field}} = AF \tag{2.3-19}$$

Alternatively, an acceleration factor is obtained for every hour from the right-hand side of Equation 2.3-7 using the calculated module temperature, relative humidity, and UV dose, and by inserting a guess value for the unknown activation energy. The average of these hourly acceleration factors should be equivalent to the acceleration factor obtained from the parameter degradation rate. By applying the appropriate Excel tool, the initial guess value for activation energy is optimized to arrive at the accepted value of activation energy for the degradation mode being considered, which, in this case, is encapsulant discoloration.

The activation energy for IMS degradation has been calculated in an analogous manner, with the differences being in the number of inputs; UV dosage is assumed to not play a role in IMS degradation.

2.3.5 UV fluorescence test

This test was conducted to visually assess the discoloration of the encapsulant in aged modules. Black light i.e. light of 350 nm wavelength was shown on individual cells of the module in a dark room and the image was captured on a regular high resolution camera. Care was taken to diffuse the light hitting the cell to avoid reflection from direct light impacting the final image.

2.3.6 EDAX test

The EDAX test was conducted to obtain information on the composition of the solder ribbon used in the construction of the modules under investigation. It was conducted on the Scanning Electron Microscopy imaging instrument at the Leroy laboratory of Solid State Physics in ASU. The solder ribbon was extracted from the back surface of the PV modules. This was done by first heating a small section of the backsheet using a hot-air gun and then carefully slicing off the heated section using a standard blade. The encapsulant was heated and sliced in an equivalent manner to expose a small section of the solder ribbon underneath which was carefully extracted using tweezers. Care was taken to ensure that the blade did not contact the solder ribbon, which could have adversely affected the SEM images.

2.4 RESULTS AND DISCUSSION

This section deals with activation energies obtained from the acceleration factors and the subsequent analysis. The analysis has been conducted for two types of degradation modes commonly observed in the field – intermetallic system degradation, and encapsulant degradation. The data for this analysis has been obtained from ASU-PTL archives and from field evaluations conducted by ASU-PRL.

The relevant details regarding the accelerated testing database are listed in table 2.4-1 below:

Table 2-2 Accelerated test (DH1000) database

No. of modules	**94**
Median Pmax degradation (%/year)	14.16
Median Rs increase (%/year)	24.89

The relevant details of the databases are listed as required within each section.

2.4.1 Intermetallic system (IMS) degradation

2.4.1.1 Identification of solder bond composition

The activation energy for IMS degradation will be dependent on the solder ribbon used during construction. In this work, three different modules were considered – BP Solar MSX, Siemens M55, and Siemens SP75. All three modules were available in ASU-PRL.

The composition of the solder bonds was ascertained through EDAX testing. The EDAX testing images have been provided below. The results are listed in table 2.4-2.

Table 2-3 Solder bond material for modules under investigation

Module type	**Solder bond composition**
SP75	Sn47Cu7Pb46
M55	Sn60Pb40
MSX	Sn60Pb40*

*Data was sourced through personal communications as the module with the exact construction was not available

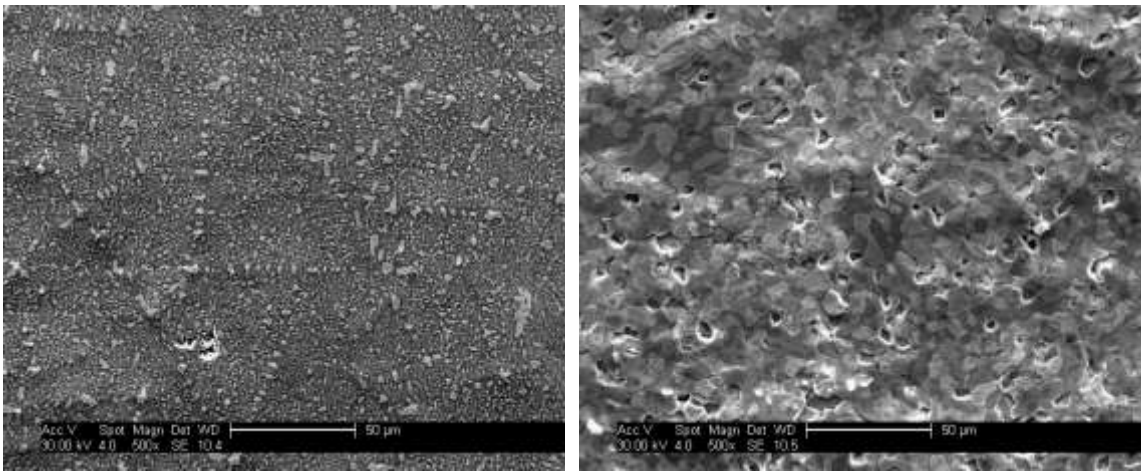

(a) (b)

Figure 2.4-1 SEM imaging of the solder ribbon extracted from (a) M55 control (b) M55 aged

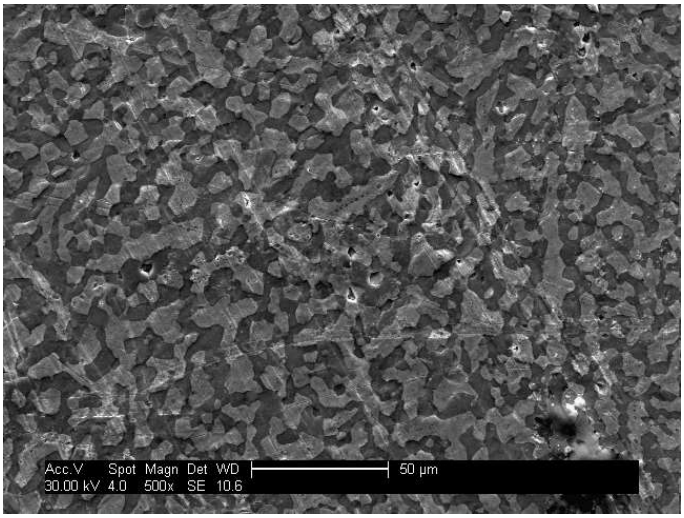

Figure 2.4-2 SEM imaging of solder ribbon extracted from aged SP75 module

2.4.1.2 Activation energy for solder bond M55

This bond type was analyzed for 3 different climate types – Arizona (hot and dry), New York (cold and humid), and Colorado (cold and dry). The modules used for this analysis were the M55 modules, the degradation patterns for which have been analyzed in a prior thesis [8]. The relevant information about these modules is listed in Table 2-4 below.

Table 2-4 Field database of M55 modules

Region	No. of modules	Median Pmax degradation (%/year)	Median Rs increase (%/year)
Arizona	3	0.58	1.96
Colorado	1	0.28	0.69
Sacramento	1	0.39	0.9

- **Activation energy in climate type: Hot and dry**

As outlined in section 2.3.3.1, the acceleration factor was obtained as the ratio of the series resistance increase of the database of modules in accelerated testing to the M55 modules recovered from the site in Arizona. The activation energy was calculated using different equations – the Arrhenius equation and Pecks equation considering ambient humidity and module humidity. Table 2-5 details the results obtained. The activation energies have been documented when considering 'No humidity' (Arrhenius equation), 'Ambient humidity', and 'Module humidity'.

Table 2-5 Activation energy for M55 in hot and dry climate type

Climate type	**Acceleration factor definition**	**AF value**	**Activation energy**		
			No humidity	**Ambient humidity**	**Module humidity**
Hot and dry	A2F	12.68	0.39	0.54	0.71

The results indicate a general increase in the activation energy required with the addition of humidity. The activation energy using module humidity is similar to the reported 0.89eV for corrosion degradation mechanism by Kimball et al [14].

Error! Reference source not found. depicts the hourly variation of the acceleration factor over one year, the average of which corresponds to the acceleration factor obtained as a ratio of the series resistance increase. As seen, the acceleration factor tends to be higher in the winters than in the summer. This is since the acceleration factor is the ratio

of the stress rate which defined using the climate conditions. In the winter, the temperatures in Arizona are far lower than the set temperature in DH1000 (i.e. 85°C), implying a much higher stress rate in the environment chamber than in the field conditions. However, in the summer, module temperatures in Arizona are quite close to the chamber temperature, resulting in similar stress rates and, subsequently, low acceleration factors.

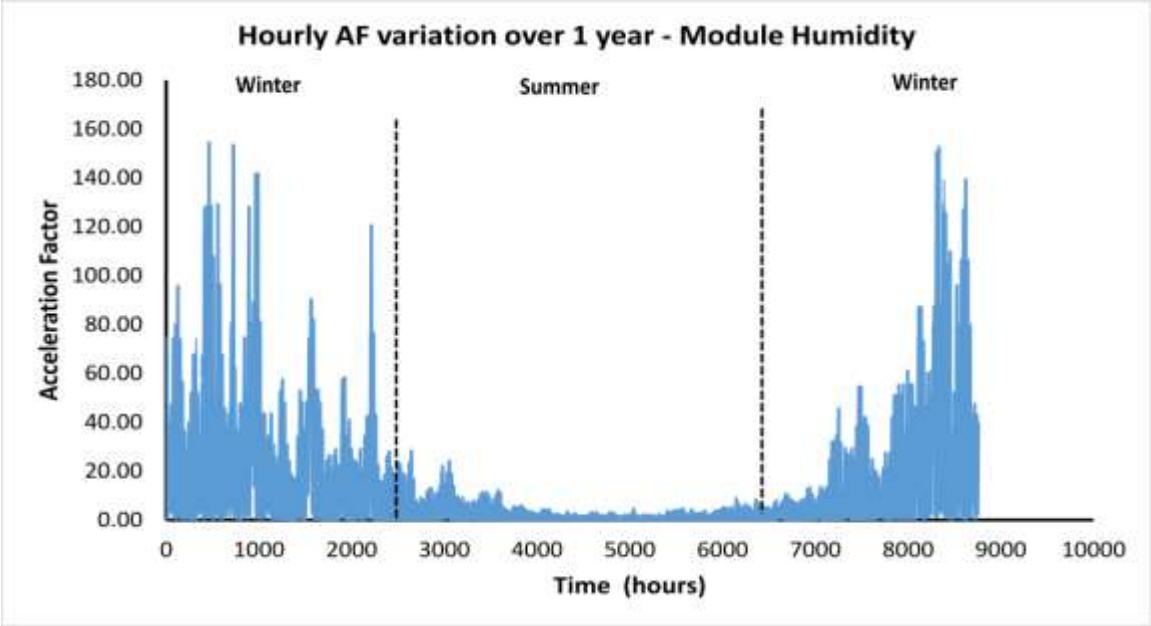

Figure 2.4-3 Annual hourly AF variation for M55 module in hot and dry climate type

- **Activation energy in climate type – Cold and dry**

The activation energy for IMS degradation in cold and dry conditions was calculated by defining the acceleration factor as A2F. The results were then cross checked with the

activation energy obtained by defining the acceleration factor as F2F to check the validity of the F2F model. The results are listed in Table 2-6.

Table 2-6 Activation energy for M55 in cold and dry climate

Climate type	Acceleration factor definition	AF value	Activation energy		
			No humidity	Ambient humidity	Module humidity
Cold and dry	A2F	36.01	0.41	0.46	0.53
	F2F	0.74	- 0.15	1.07	0.78

The A2F results indicate the activation energy for IMS degradation in cold and dry regions is ranging from 0.4 to 0.55 depending on the model. The variation of the acceleration over one year is depicted in Figure 2.4-4.

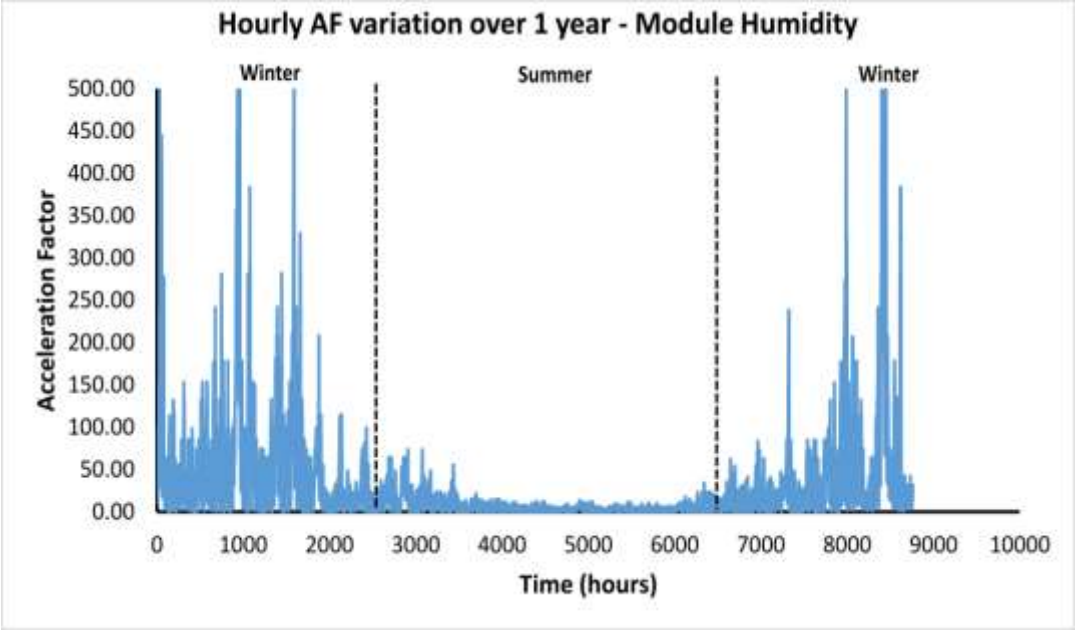

Figure 2.4-4 Annual hourly AF variation for M55 module in cold and dry climate

As was the case with the variation in Figure 2.4-3, the acceleration factor is higher in the winters than in the summer due to higher stress rates in the winter conditions. A point to note is that the range of the acceleration factor is much higher in comparison to Arizona, since temperatures drop much lower in Golden, Colorado than they do in Phoenix, Arizona. The plot also throws up a few outliers where the acceleration factor has reached extremely high values. These are regions where the temperature in the field had fallen 30 ^{o}C below zero, possibly due to a blizzard, or an imperfect measurement by the station, and as such, will be ignored for this analysis.

The F2F analysis does not seem to yield acceptable values for the activation energy. The Arrhenius model results in a negative activation energy, implying that this model is invalid for this analysis. The activation energy obtained through the module humidity model is close to the accepted value, but the high value from the ambient humidity model suggests that the models may not be very stable for comparing these climate types. One probable reason for this is the data under consideration. The module data set comprises the best 3 out of 12 modules from Arizona while only 1 module from Colorado, leaving little margin for error in the case of Colorado. It is possible that the Colorado dataset may not be entirely representative of the effects of weather stresses in that region due to a prior unobserved manufacturing defect. Hence, a low statistical sampling rate for both regions may have compounded the error to yield a seemingly faulty variation as depicted in Figure 2.4-5.

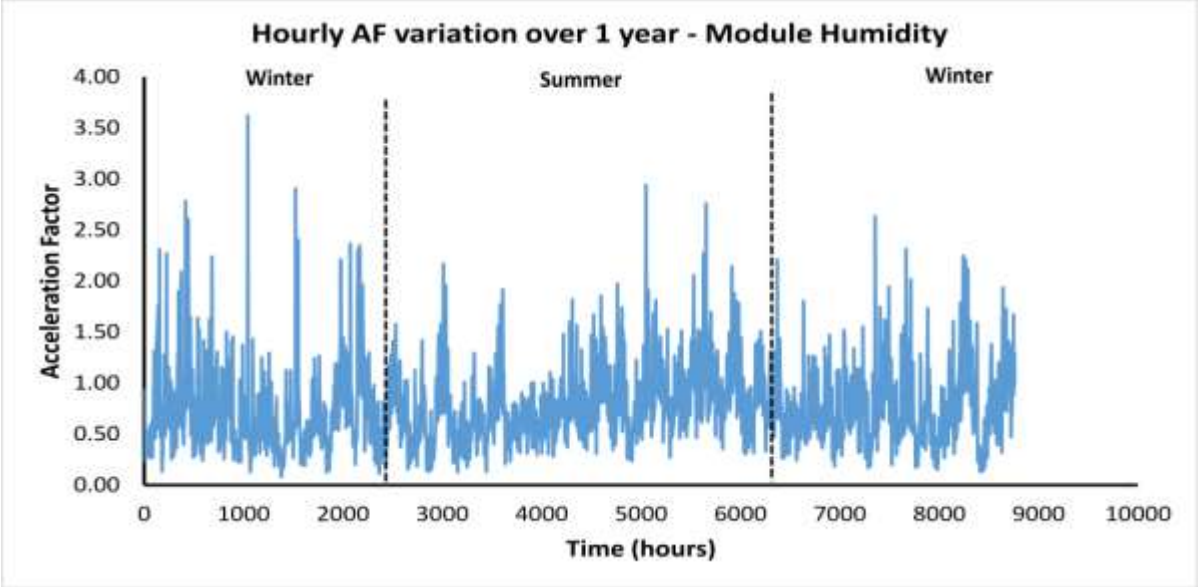

Figure 2.4-5 Annual hourly AF variation (F2F) for M55 module in cold and dry climate

- **Activation energy in climate type – Hot and humid**

As with the previous climate type, the activation energy for IMS degradation was obtained by defining acceleration factor as A2F and, subsequently, compared with the results obtained through F2F. This analysis was conducted on an M55 module recovered from a power plant in Sacramento, California. The performance and reliability characterization for this module was done in a prior thesis work.[8] and the results of this work can be found in Table 2-7.

Table 2-7 Activation energy for M55 module in hot and humid climate

Climate type	Acceleration factor definition	AF value	Activation energy		
			No humidity	Ambient humidity	Module humidity
Hot and humid	A2F	27.73	0.43	0.45	0.59
	F2F	0.74	- 0.13	Does not fit*	Does not fit*

*Does not fit implies that the model could not generate an activation energy value which would result in the acceleration factor value observed

The A2F model indicates an activation energy ranging from 0.4-0.6eV, which is similar to the range for cold and dry conditions. Figure 2.4-6 depicts a satisfactory acceleration factor variation over one year, with the factor values higher in the winter than in the summer as is expected.

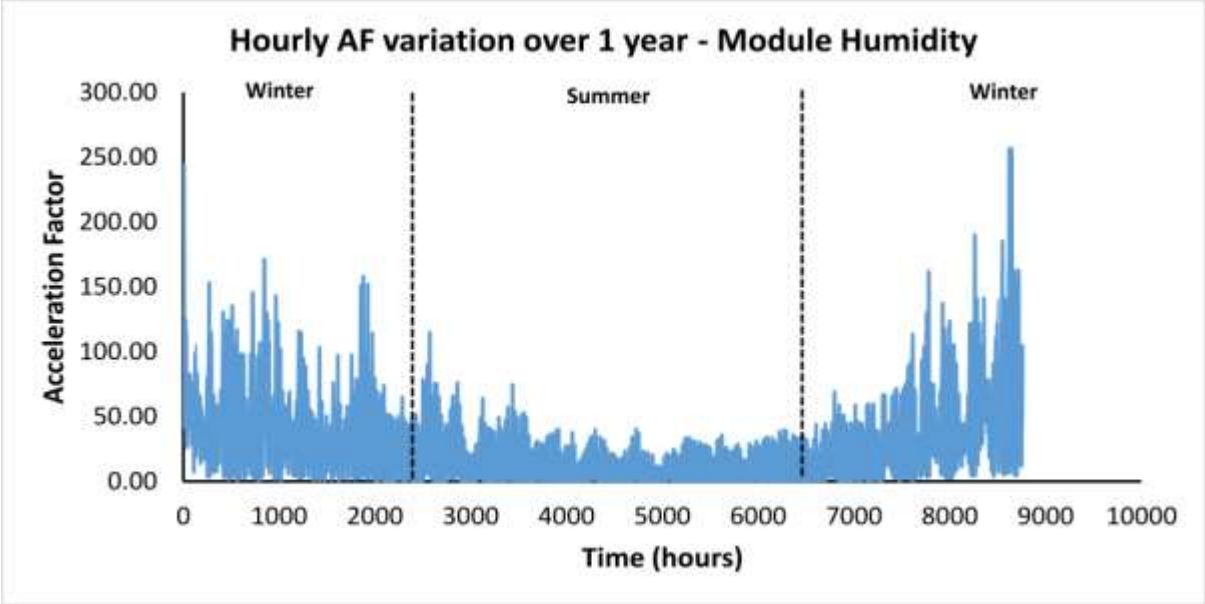

Figure 2.4-6 Annual hourly AF variation (A2F) for M55 module in hot and humid climate

However, the F2F model did not fit for the observed ratio of Rs increase %. The model limitations may have risen due to unavailability of statistically backed data as only one module from the California site was used in this analysis. Another reason, which cannot be ruled out, is the inapplicability of using a field to field acceleration factor.

2.4.1.3 Analysis of model accuracy for M55 solder bond

The activation energy for IMS degradation for the M55 solder bond was obtained by considering different humidity levels. The results obtained have been listed in *Table 2-8*.

The Arrhenius model indicates an activation energy centered at 0.42 eV.

The Pecks model with ambient humidity yields a similar result with the activation energy ranging from 0.45 – 0.54eV. The extent of this range is mirrored in the model with module humidity, with the activation energy ranging from 0.5 – 0.7eV. The geoplot analysis in Figure 2.4-7 shows the variation in activation energy, when going from a low level to a high level of temperature on the x axis and, when going from a low level to a high level of relative humidity on the y axis.

Table 2-8 Summary of activation energy for M55 modules in different climate types

Climate type	Acceleration	Activation energy (eV)

	Factor		No humidity		Ambient humidity		Module humidity	
	A2F	**F2F**	**A2F**	**F2F**	**A2F**	**F2F**	**A2F**	**F2F**
Hot and dry	12.68	NA	0.39	NA	0.54	NA*	0.71	NA*
Hot and humid	27.73	0.96	0.43	-0.13	0.45	No fit**	0.59	No fit**
Cold and dry	36.01	0.74	0.41	-0.15	0.46	1.07	0.53	0.78

* NA since the hot and dry climate type was considered as the reference for the F2F modelling

** No fit implies no guess value of activation energy could result in the observed AF

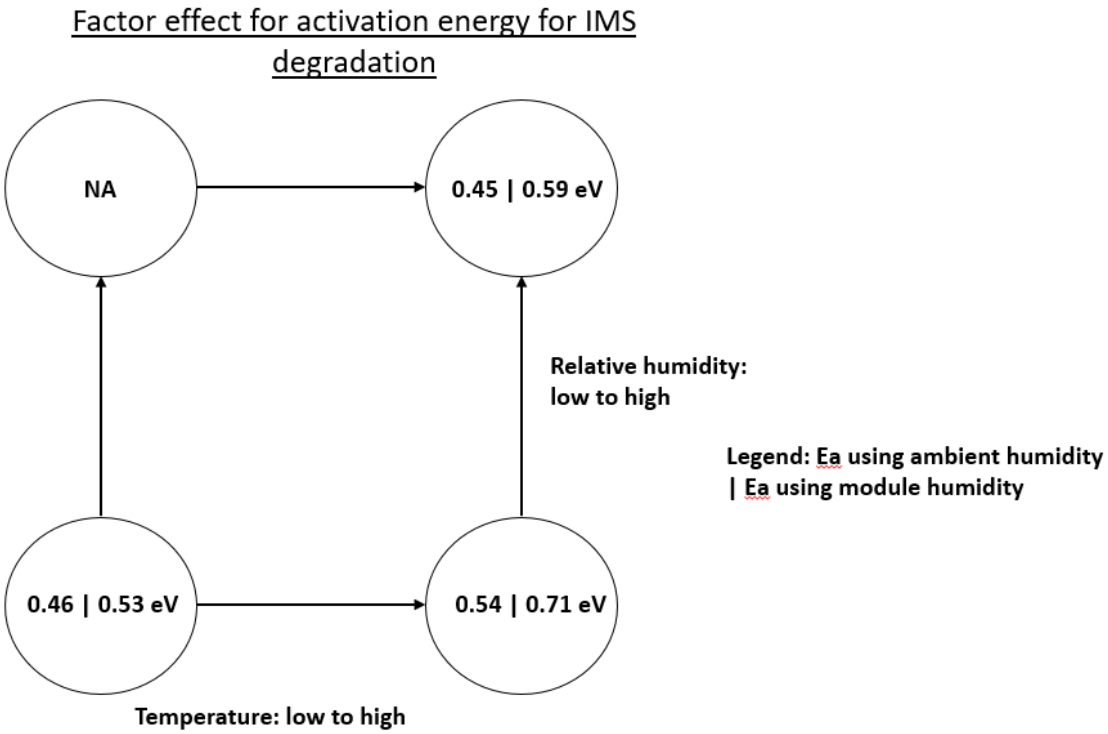

Figure 2.4-7 Geoplot analysis of activation energy using Pecks model

The plot seems to indicate an increase in the activation energy value going from a region of low temperature to a hot region of high temperature. It is also interesting to note the drop in activation energy going from a region of high humidity to a region of lower humidity, indicating that relative humidity is playing a role in IMS degradation. However, this temperature and relative humidity dependence is subject to the accuracy of dataset of the Colorado region.

2.4.1.4 Activation energy of solder bond MSX

The activation energy for IMS degradation for this solder bond type was conducted by analyzing two climate types. The details regarding the modules and the series resistance increase values is listed in Table 2-9.

Table 2-9 Field database of MSX modules

Region	No. of modules	Median Pmax degradation (%/year)	Median Rs increase (%/year)
Arizona	6	0.56	1.11
New York	2	0.62	0.93
New York	132	0.66	0.43

Conducting a preliminary analysis, the median Pmax degradation values indicate a surprising trend of a higher degradation rate in New York when compared to the degradation rate in Arizona. However, this trend disappears in the case of median Rs increase %. This seems to further the case being made in this thesis that different degradation modes can account for the Pmax degradation and, hence, it is important to go one step deeper and investigate based on the parameter directly affected by the degradation mode.

- **Activation energy for climate type – hot and dry**

The activation energy for IMS degradation for the MSX solder bond in the hot and dry climate type was calculated using the Arizona module dataset. The results listed below in Table 2-10 were obtained by defining acceleration factor as A2F.

Table 2-10 Activation energy for MSX module in hot and dry climate

Climate type	Acceleration factor defined as	AF value	Activation energy		
			No humidity	Ambient humidity	Module humidity
Hot and dry	A2F	22.43	0.47	0.61	0.79

The Arrhenius model yields an activation energy of 0.47eV, which is similar to the activation energy for the M55 solder bond obtained by using this same model. The Pecks model yields an activation energy ranging from 0.6 – 0.8 eV depending on the humidity values being considered. Looking at the annual hourly AF variation in Figure 2.4-8, it indicates a similar trend with higher acceleration factors in the winter than in the summer.

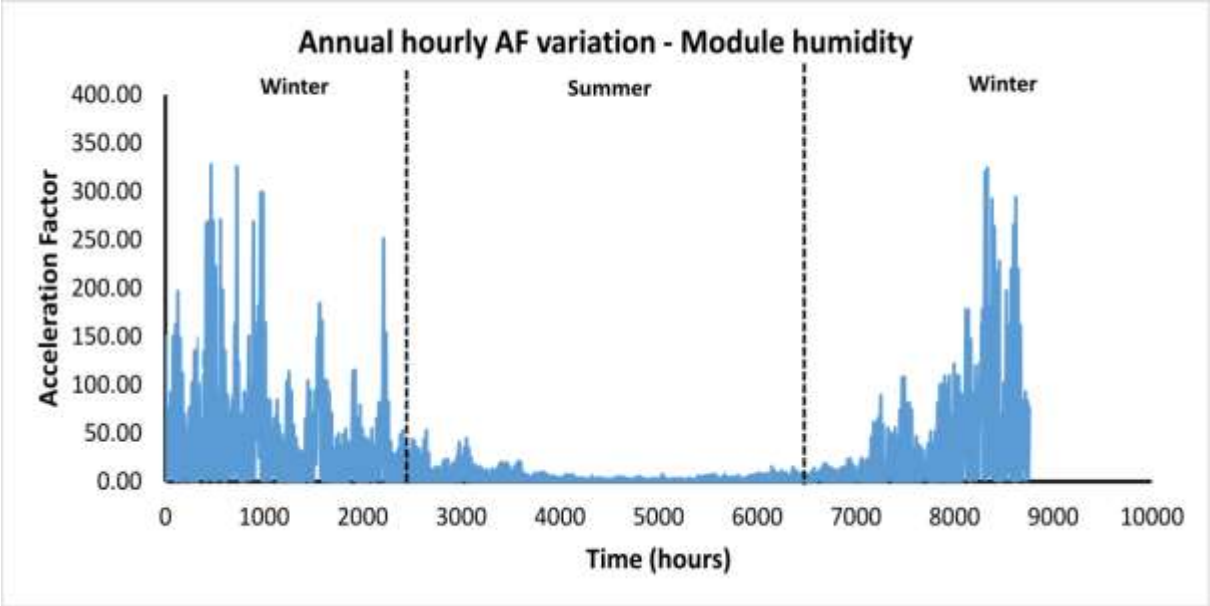

Figure 2.4-8 Annual hourly AF variation for MSX module in hot and dry climate

- **Activation energy in climate type – cold and humid**

The activation energy for IMS degradation in cold and humid climate was calculated using the New York datasets. 2 modules were recovered from the 132 modules evaluated at the site itself. However, the high value of Rs increase % of those two modules in comparison with the power plant median (0.93% v/s 0.43%) suggests that those two modules may not be indicative of the median Rs increase observed in New York. For convenience, the two sets of data will be referred to as NY2 (2 modules) and NY132 (132 modules). The results, detailed below in Table 2-11, were compiled by considering both definitions of acceleration factor.

Table 2-11 Activation energy for MSX module in cold and humid climate

Code	Acceleration factor defined as	AF value	Activation energy		
			No humidity	Ambient humidity	Module humidity
NY2	A2F	26.89	0.40	0.47	0.46
	F2F	1.20	- 0.10	1.58	1.71
NY132	A2F	57.93	0.49	0.55	0.54
	F2F	2.58	0.47	0.88	0.83

The Arrhenius model suggests an activation energy ranging between 0.4-0.5 eV. It increases marginally when considering Pecks model. Figure 2.4-9 indicates a typical variation in the annual hourly acceleration factor with a couple of outliers. Delving deeper, these outliers were from cases where the module relative humidity was higher than 100%, explainable by supersaturation phenomenon commonly observed in calculation models for relative humidity.

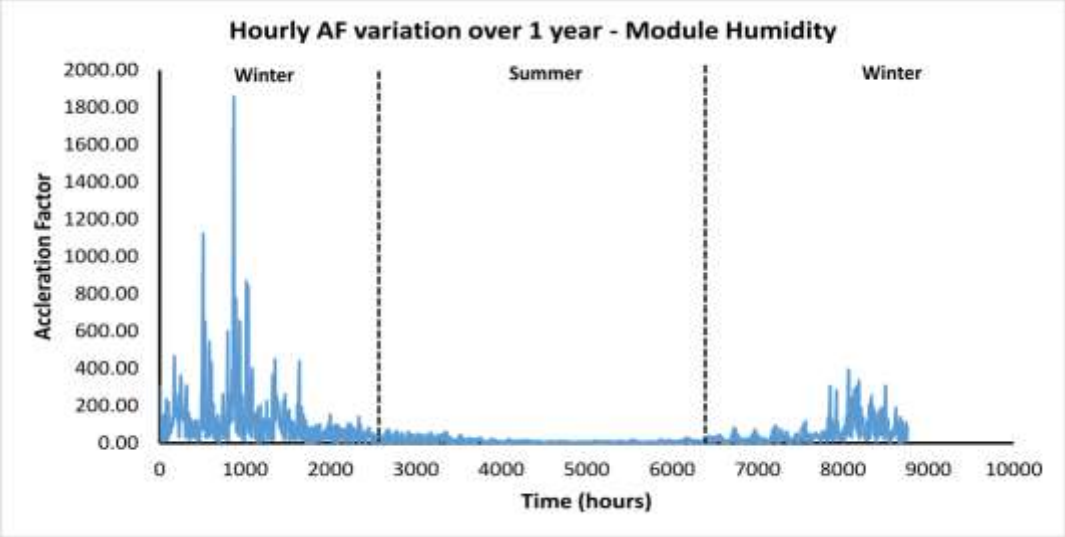

Figure 2.4-9 Annual hourly AF variation for MSX module in cold and humid climate

The F2F model seems to work better in the case of NY132, yielding slightly higher values than those that are expected. The variation in the annual hourly AF, depicted in Figure 2.4-10 indicates slightly higher AF values in the summer than in the winter as stress levels in the summer in Arizona will be higher than those in New York. However, this is counter balanced by the higher relative humidity in New York as compared to Arizona during the summer, resulting in narrow range band.

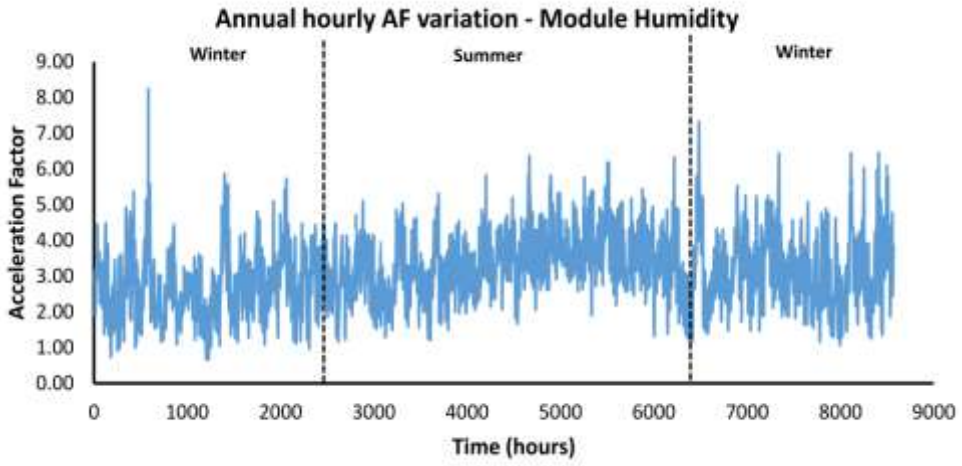

Figure 2.4-10 Annual hourly AF variation (F2F) for MSX module in cold and humid climate

2.4.1.5 Analysis of model accuracy for solder bond MSX

Table 2-12 Summary of activation energy results for MSX modules in different climate types

Climate type	Acceleration Factor		Activation energy (eV)					
			No humidity		Ambient humidity		Module humidity	
	A2F	F2F	A2F	F2F	A2F	F2F	A2F	F2F
Hot and dry	22.43	NA	0.47	NA	0.61	NA	0.79	NA
Cold and humid	57.93	2.58	0.49	0.47	0.55	0.88	0.54	0.88

It is interesting to note that the Arrhenius model has consistently maintained an activation energy ranging between 0.4-0.5 eV for both solder bonds, apart from two outliers. The

activation energy using Pecks model is between 0.5 – 0.6 eV for IMS degradation using the A2F model while it jumps up to 0.88 eV for the F2F model, suggesting model irregularities.

2.4.1.6 Activation energy of solder bond SP75

The activation energy for IMS degradation in this case was calculated using field evaluation data from a site in Arizona. The details of the modules are listed in Table 2-13

Table 2-13 Field database for SP75 modules

Region	No. of modules	Median Pmax degradation (%/year)	Median Rs increase (%/year)
Arizona	252	1.23	1.90

The results for activation energy for IMS degradation in hot and dry climate, listed in

Table 2-14 were obtained by defining the acceleration factor as A2F.

Table 2-14 Activation energy for SP75 modules in hot and dry climate

Climate type	Acceleration factor defined as	AF value	Activation energy		
			No humidity	Ambient humidity	Module humidity
Hot and dry	A2F	13.13	0.40	0.54	0.73

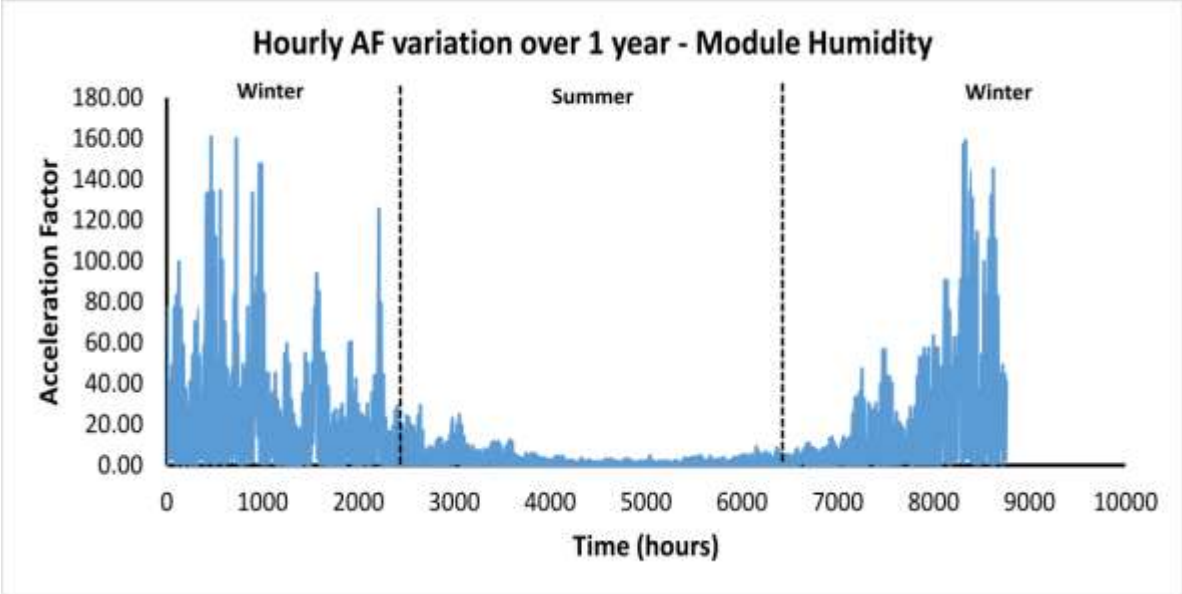

Figure 2.4-11 Annual hourly AF variation for SP75 modules in hot and dry climate

2.4.1.7 Discussion of results for activation energy of IMS degradation

Figure 2.4-12 indicates the range of activation energy for the $Sn_{60}Pb_{40}$ solder bond type in the two different module constructions, MSX and M55 based on the A2F model. The

results indicate that the consideration of relative humidity to the model increases the activation energy. Between the two Peck's models, the activation energy values are higher for the module humidity model as this model will take more time to equilibrate. It is also interesting to note that the MSX modules have slightly higher activation energies than the M55 modules. This could be due to the 2% Ag addition in the solder bond composition of the MSX module, the addition being primarily to hinder the formation of the lead-silver ternary alloy.

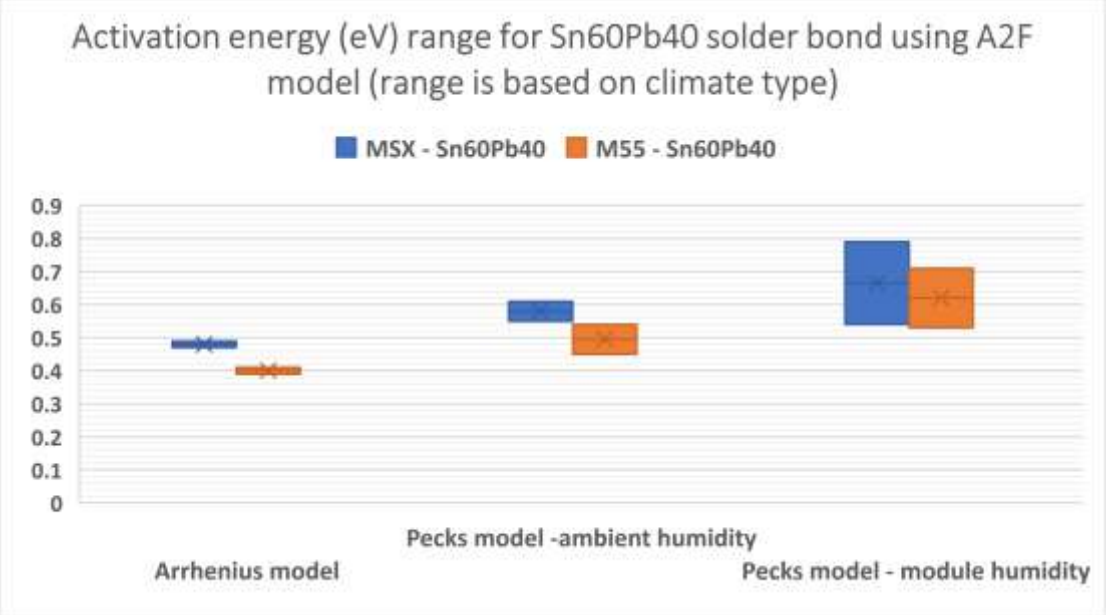

Figure 2.4-12 Activation energy range for Sn60Pb40 solder bond using A2F model

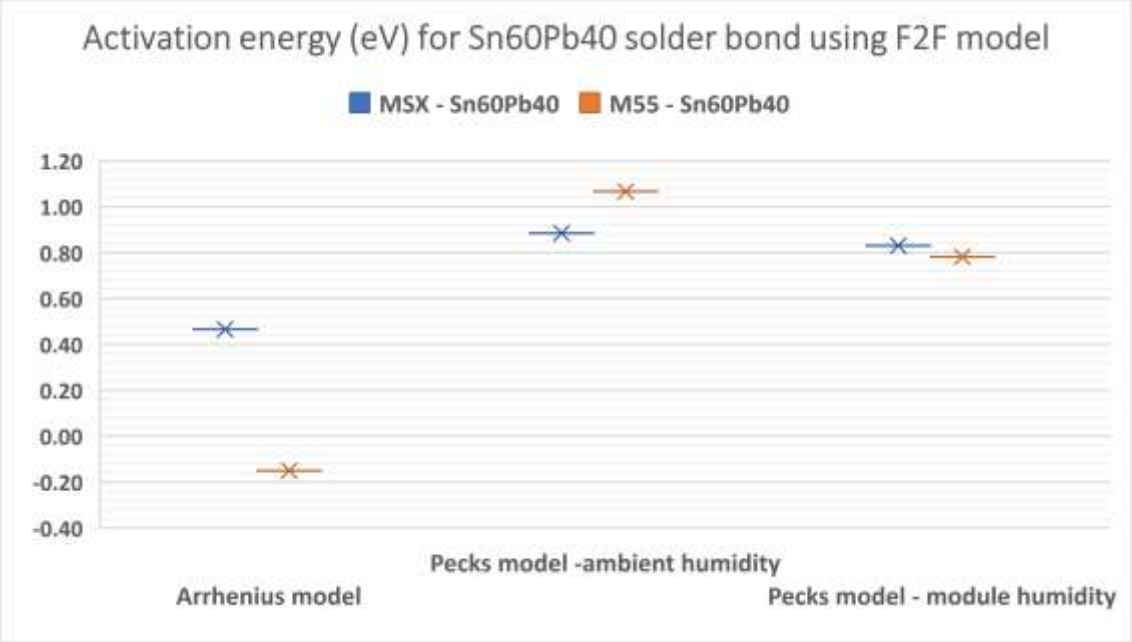

Figure 2.4-13 Activation energy range for Sn60Pb40 solder bond using F2F model

The activation energy values obtained using the Arrhenius model are slightly lower than the ones reported by Geipel et al [13] who also used an Arrhenius model. This could be because series resistance could be impacted due to IMC formation and thermal fatigue. Presently, since our model does not consider the thermal fatigue component, it attributes the series resistance increase entirely to the IMC formation, thereby yielding a lower activation energy requirement for this degradation mode. The addition of a thermal fatigue component, as modelled by Bosco et al [12] could drive up the activation energy requirement for IMC formation as its overall influence on series resistance increase will be reduced.

2.4.2 Activation energy for encapsulant degradation

For encapsulant degradation, the parameter focused on is Isc degradation. The results have been analyzed under the assumption that minor variation in the encapsulant composition does not overtly change the activation energy for its degradation.

The acceleration factor has been defined as F2F, where it has been modelled as the ratio of Isc degradation in Arizona to the Isc degradation in the other climate types.

The parameters for the modules used for in this analysis have been detailed in Table 2-15. As described in section 2.3.3.2, this analysis includes modified Pecks equation and the modified Arrhenius equation.

Table 2-15 Field database for modules used in encapsulant degradation analysis

Region	Module type	No. of modules	Median Pmax degradation (%/year)	Median Isc degradation (%/year)
AZ | NY	MSX	6 | 2	0.56 | 0.66	0.43 | 0.59
AZ | CO	M55	3 | 1	0.96 | 0.28	0.23 | 0.31

The activation energies have been obtained for two climate types – cold and humid (NY) and cold and dry (CO) when compared with the degradation pattern in Arizona. The results for encapsulant degradation have been detailed in Table 2-15 below, with the models defined in the following manner:

- Arrhenius equation: f (T)
- Modified Pecks equation: f (T, UV, $RH_{ambient/module}$)
- Modified Arrhenius equation: f (T, UV)

Table 2-16 Activation energy results for encapsulant degradation

F2F regions	**AF value**	**Activation energy**			
		f (T)	**f (T, UV, RH_{amb})**	**f (T, UV, RH_{mod})**	**f (T, UV)**
AZ | NY	0.73	-0.16	1.83	2.28	0.31
AZ | CO	0.74	-0.15	1.11	0.92	0.29

The Arrhenius model yields negative activation energies for both regions, indicating that this model may not be applicable for this degradation mode. Similarly, the activation energies yielded through Pecks modified equations are much higher than expected. The modified Arrhenius equation results in activation energies centered around 0.3 eV, which is close to the accepted value. Figure 2.4-14 and Figure 2.4-15 indicates the day-time hourly variation of acceleration factors. Since the modules will be exposed to UV light only during the day, it makes sense to look at the acceleration factors only during day time.

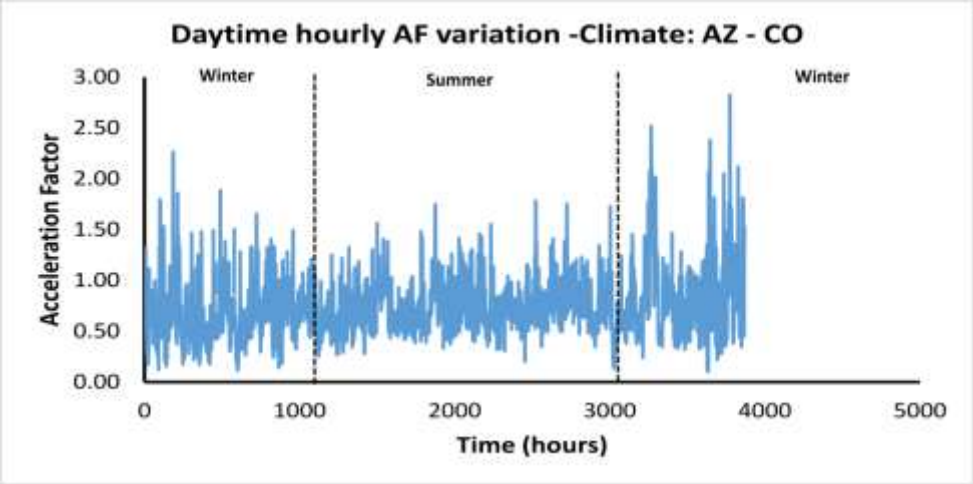

Figure 2.4-14 Annual day-time AF variation for cold and dry climate type

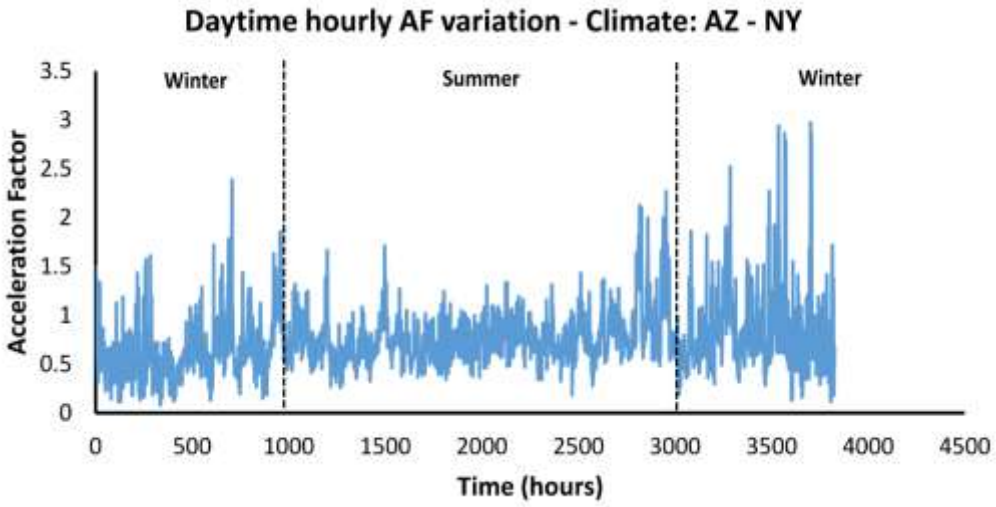

Figure 2.4-15 Annual day-time AF variation for cold and humid climate type

The plots indicate a marginal increase in acceleration factors over the winter as compared to summer. This is since Arizona will receive more UV light in the winter as compared to Colorado and New York.

2.4.2.1 Discussion on the impact of oxygen bleaching

Oxygen bleaching seems to play an important role in encapsulant degradation. At present, the model does not account for the impact of oxygen bleaching, resulting in incorrect results where bleaching has affected the Isc. Hence, the AF equation needs to be of the form as outlined below:

$$AF = discoloration\ reaction - oxygen\ bleaching\ reaction \quad (2.4\text{-}1)$$

The rate of oxygen difusion can play a significant role in the rate of oxygen bleaching. A reasonable understanding can be obtained through the pattern of browning obtained through UV fluorescence imaging of the MSX modules. The browning seems to be in between the bus bars of the AZ modules while it covers a larger surface area in New York. This can be attributed to the rate of diffusion of oxygen, with the modules from Arizona having a higher rate due to higher average temperatures than New York.

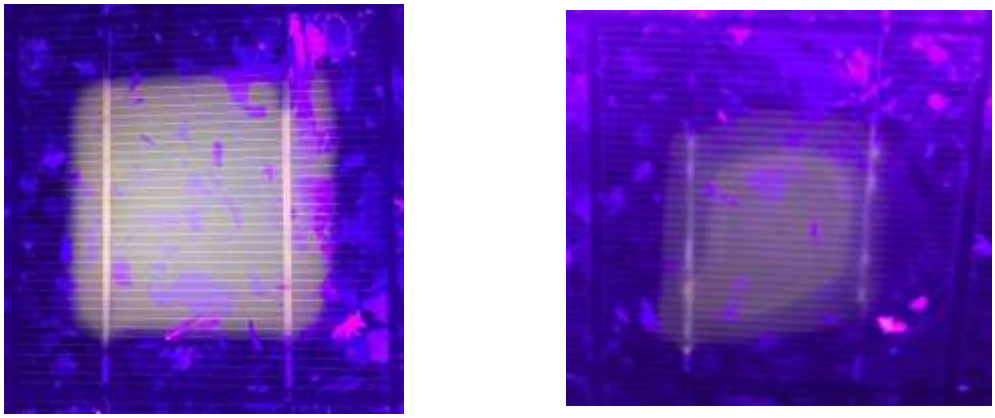

(a) (b)

Figure 2.4-16 UV fluorescence imaging for module in (a) Arizona and (b) New York

To model the rate of oxygen bleaching, it is important to understand whether this reaction is mass transfer controlled or reaction controlled i.e. whether it is to be modelled as per Fickian law or reaction equilibrium law. As seen in the figures above, oxygen seems to diffuse from the sides of the cells towards the center, indicating that the bleaching reaction occurs as far as the oxygen diffuses through the encapsulant. This suggests that the reaction is, in fact, mass transfer controlled and attempts can be made to model it as per Fickian Law. The acceleration factor for oxygen bleaching could be modelled as a function of the ratio of the oxygen concentration gradient in the encapsulant from the side of the cell to the center of the cell:

$$AF = \frac{D_{e1}\frac{\partial C_1}{\partial x}}{D_{e2}\frac{\partial C_2}{\partial x}} \tag{2.4-2}$$

Where: $\mathrm{D_e} = \mathrm{D_o}\exp\left(\frac{-\mathrm{Ea}}{\mathrm{kT}}\right)$; with $\mathrm{D_o}$ being the mass transfer coefficient for oxygen in the encapsulant and '1' and '2' are the two climate types under consideration

Leading to the following expression for encapsulant time-to-failure:

$$AF = exp\left(\frac{-Ea}{k}\left(\frac{1}{T_{AZ}} - \frac{1}{T_{field}}\right)\right)\left(\frac{RH_{AZ}}{RH_{field}}\right)^n\left(\frac{UV_{AZ}}{UV_{field}}\right)^m \pm \frac{D_{o1}}{D_{o2}}exp\left(\frac{-Ea}{k}\left(\frac{1}{T_1} - \frac{1}{T_2}\right)\right)\frac{\frac{\partial C_1}{\partial x}}{\frac{\partial C_2}{\partial x}} \tag{2.4-3}$$

The AF values obtained presently are less than 1, indicating that, contrary to the accepted notion, the rate of encapsulant degradation is lesser in Arizona than in Colorado/New York. This inherent logic of Equation 2.3-14 could be the cause for the high activation

energies presently obtained. Introducing the oxygen bleaching component, as seen in Equation 2.4-3, could account for the higher rate oxygen bleaching in Arizona, as compared to New York/Colorado, and drive down the activation energies to the accepted value.

2.5 CONCLUSIONS

The objective of this work was to identify the performance parameter directly affected by a climatic degradation mode and model its degradation as a function of the combination of the three primary climate factors: T, RH, and UV. The combination of these factors resulted in different models, all of which were validated through comparison of the activation energy obtained with that reported in literature. The following conclusions can be drawn through the results:

1. IMS degradation directly affects the series resistance while encapsulant degradation impacts the short circuit current.
2. The activation energy for IMS degradation was calculated through two models – A2F and F2F. For each model, different functions were considered. Although the idea of the F2F model has been introduced as a way to replace accelerated testing data requirement for time to failure modelling, it will require larger datasets for reliable results. At present, its close association with the results of the A2F model indicated its validity of use in encapsulant degradation modelling. The A2F model yielded activation energies in the range of 0.4 – 0.8eV based on the climate type for the $Sn_{60}Pb_{40}$ solder bond. As discussed in Section 2.4.1.7, this value is expected to increase once the thermal fatigue component is added to the model. At present, the IMS degradation has been modelled as:

$$\frac{\text{Rs increase rate}_{\text{Acc}}}{\text{Rs increase rate}_{\text{field}}} = \text{AF} = \exp\left(\frac{-(0.4-0.8\text{eV})}{\text{k}}\left(\frac{1}{\text{T}_{\text{Acc}}}-\frac{1}{\text{T}_{\text{field}}}\right)\right)\left(\frac{\text{RH}_{\text{Acc}}}{\text{RH}_{\text{field}}}\right)^{-2.2}$$

3. The activation energy for encapsulant browning was calculated using the F2F model. Numerous functions were considered with combinations of T, UV and RH. The results indicated that the Modified Arrhenius model (f(T,UV)) i.e. Equation 2.3-15 was the best fit as the activation energy yielded was 0.3eV which was close to the value reported in literature[17]. However, this was probably since the model does not consider the impact of oxygen bleaching. It is possible that the addition of such a term may result in the Modified Pecks equation (f(T, UV, RH)) being the best fit. As such, at present, the equation below was the best fit:

$$\frac{Isc\ degradation_{AZ}}{Isc\ degradation_{field}} = AF = exp\left(\frac{-0.3eV}{k}\left(\frac{1}{T_{AZ}} - \frac{1}{T_{field}}\right)\right)\left(\frac{UV_{AZ}}{UV_{field}}\right)^{0.6}$$

REFERENCES

[1] S. Shrestha, "Determination of Dominant Failure Modes Using Combined Experimental and Statistical Methods and Selection of Best Method to Calculate Degradation Rates," ARIZONA STATE UNIVERSITY, 2014.

[2] A. Birolini, *Quality and Reliability of Technical Systems: Theory, Practice, Management*. Springer, 2004.

[3] M. Lazzaroni, L. Cristaldi, L. Peretto, P. Rinaldi, and M. Catelani, *Reliability Engineering: Basic Concepts and Applications in ICT*. Springer, 2012.

[4] J. Bowles, "An Assessment of RPN Prioritization in a Failure Modes Effects and Criticality Analysis," vol. 47, no. 1, p. 51, 2004.

[5] J. M. Kuitche, R. Pan, and G. TamizhMani, "Investigation of Dominant Failure Mode(s) for Field-Aged Crystalline Silicon PV Modules Under Desert Climatic Conditions," *IEEE J. Photovolt.*, vol. 4, no. 3, pp. 814–826, May 2014.

[6] "NSRDB: 1991- 2005 Update: TMY3." [Online]. Available: http://rredc.nrel.gov/solar/old_data/nsrdb/1991-2005/tmy3/. [Accessed: 23-Mar-2017].

[7] M. K. Moorthy, "Automation of Risk Priority Number Calculation of Photovoltaic Modules and Evaluation of Module Level Power Electronics," ARIZONA STATE UNIVERSITY, 2015.

[8] M. Chicca, "Characterization and Analysis of Long Term Field Aged Photovoltaic Modules and Encapsulant Materials," ARIZONA STATE UNIVERSITY, 2015.

[9] F. J. Pern and A. W. Czanderna, "Characterization of ethylene vinyl acetate (EVA) encapsulant: Effects of thermal processing and weathering degradation on its discoloration," *Sol. Energy Mater. Sol. Cells*, vol. 25, no. 1–2, pp. 3–23, 1992.

[10] M. Köntges, S. Kurtz, C. Packard, U. Jahn, K. A. Berger, and K. Kato, *Performance and reliability of photovoltaic systems: subtask 3.2: Review of failures of photovoltaic modules: IEA PVPS task 13: external final report IEA-PVPS*. Sankt Ursen: International Energy Agency, Photovoltaic Power Systems Programme, 2014.

[11] G. R. Mon, L. C. Wen, R. S. Sugimura, and R. G. Ross, “Reliability studies of photovoltaic module insulation systems,” in *Proceedings of the 19th Electrical Electronics Insulation Conference,* 1989, pp. 324–329.

[12] N. Bosco, T. J. Silverman, and S. Kurtz, “Climate specific thermomechanical fatigue of flat plate photovoltaic module solder joints,” *Microelectron. Reliab.*, vol. 62, pp. 124–129, Jul. 2016.

[13] T. Geipel, M. Moeller, J. Walter, A. Kraft, and U. Eitner, “Intermetallic compounds in solar cell interconnections: Microstructure and growth kinetics,” *Sol. Energy Mater. Sol. Cells*, vol. 159, pp. 370–388, Jan. 2017.

[14] G. M. Kimball, S. Yang, and A. Saproo, “Global acceleration factors for damp heat tests of PV modules,” in *Photovoltaic Specialists Conference (PVSC), 2016 IEEE 43rd*, 2016, pp. 0101–0105.

[15] M. Koehl, M. Heck, and S. Wiesmeier, “Modelling of conditions for accelerated lifetime testing of Humidity impact on PV-modules based on monitoring of climatic data,” *Sol. Energy Mater. Sol. Cells*, vol. 99, pp. 282–291, Apr. 2012.

[16] A. P. Dobos, “An Improved Coefficient Calculator for the California Energy Commission 6 Parameter Photovoltaic Module Model.” Journal of Solar Engineering, May-2012.

[17] D. J. V. Kumar, “Determination of Activation Energy for Encapsulant Browning of Photovoltaic Modules,” Arizona State University, 2016.